Review

Combustion Synthesis of MAX Phases: Microstructure and Properties Inherited from the Processing Pathway

Sofiya Aydinyan [1,2]

1   A.B. Nalbandyan Institute of Chemical Physics NAS RA, P. Sevak 5/2, Yerevan 0014, Armenia;
    sofiya.aydinyan@taltech.ee
2   Department of Mechanical and Industrial Engineering, Tallinn University of Technology, Ehitajate tee 5,
    19086 Tallinn, Estonia

Abstract: The MAX phases exhibit outstanding combination of strength and ductility which are unique features of both metals and ceramics. The preparation of pure MAX phases has been challenging due to the thermodynamic auspiciousness of intermetallic formation in the ternary systems. This review demonstrates the power of the self-propagating, high-temperature synthesis method, delivers the main findings of the combustion synthesis optimization of the MAX phases, and reveals the influence of the combustion wave on the microstructure features thereof. The possibility of using elements and binary compounds as precursors, oxidizers, and diluents to control the exothermicity was comparatively analyzed from the point of view of the final composition and microstructure in the following systems: Ti-Al-C, Ti-V-Al-C, Cr-V-Al-C, Ti-Cr-Al-C, Ti-Nb-Al-C, Ti-Al-Si-C, Ti-Al-Sn-C, Ti-Al-N, Ti-Al-C-N, Ti-Al-B, Ti-Si-B, Ti-Si-C, Nb-Al-C, Cr-Al-C, Cr-Mn-Al-C, V-Al-C, Cr-V-Al-C, Ta-Al-C, Zr-S-C, Cr-Ga-C, Zr-Al-C, and Mo-Al-C, respectively. The influence of sample preparation (including the processes of preheating, mechanical activation, and microwave heating, sample geometry, porosity, and cold pressing) accompanied with the heating and cooling rates and the ambient gas pressure on the combustion parameters was deduced. The combustion preparation of the MAX phases was then summarized in chronological order. Further improvements of the synthesis conditions, along with recommendations for the products quality and microstructure control were given. The comparison of the mechanical properties of the MAX phases prepared by different approaches was illustrated wherever relevant.

Keywords: self-propagating high-temperature synthesis; combustion synthesis; MAX phases; microstructure; mechanical properties

1. Introduction

Research on MAX phases have only gained a significant level of attention recently following on from 40 years of their discovery by Nowotny and coworkers [1], as in the 1990s researchers reported on the unique mechanical properties combined with their high resistance to oxidation and the aggressive environments of the Ti_3SiC_2 soft ceramic synthesized using the self-propagating high temperature synthesis [2] and reactive hot-pressing methods [3]. MAX phases are defined as curious class of layered hexagonal materials with general formula of $M_{n+1}AX_n$, where n = 1–3, M represents an early transition metal (specifically, a metal from groups 3–7), A is an A-group element (specifically a subset of elements from 13–16), and X is carbon and/or nitrogen. Since then, phases with multiple M and A site elements, as well as with higher "n" values have also been uncovered within the MAX family, such as 523 phases, 615 phases, or 725 phases, respectively, in addition to MAB borides (where the potential X-element is boron, as predicted from DFT calculations) [4]. More than 5000 papers have been published in the past biennium (in the period of 2022–2023, whereby a Google Scholar search was performed on 28 June 2023 with the keyword "MAX phase" in the title), offering new compositions with a tuned structure

and unusual properties of MAX derivatives (MXene) for electrocatalytic applications; however, the complexity of regulation phase composition and their diverse microstructure compels researchers to survey new pathways for their fabrication [5]. Commercially available MAX phases have already been deemed as expensive due to their expensive precursor powders, low demand, and technological hurdles. For example, Sandwik Heating Technology in Sweden currently sell Ti_2AlC and Ti_3SiC_2 powders and bulks at prices of 500 EUR/kg targeted for high-temperature applications [6]. When comparing the synthesis methods of metals, ceramics, and composites, self-propagating high-temperature synthesis (SHS) or combustion synthesis (CS) takes advantage over most of them due to energy efficiency, affordable precursors, self-sustaining exothermic reaction of wide control, productivity and self-purification behavior, and the simplicity of the equipment used [7,8]. SHS provides a vast variety of product shapes and dimensions, from films to porous structures, powders, or high density bulks. In addition, easy scale-up is characteristic to combustion synthesis [9]. The development of these novel SHS pathways from the currently available oxide precursors will lead to a significant reduction in the price required for the industrial preparation of these MAX phases.

The aim and motivation of this review was to confer the regulation of the combustion wave and optimization strategies of pure MAX phase preparation using the currently available or more affordable precursors. In addition, the salient features of SHS-produced MAX phases from different precursors, and further benefits or perspectives of combining these MAX phases with metals, ceramics, or their further extension to high-entropy MAX phases were also delivered.

2. Precursors, Preparation of Green Bodies, Combustion Parameters, and Phase Composition

2.1. SHS from Elements

The main strategies include the usage of elements as precursors; some works suggest the utilization of oxides and binary compounds containing components of the MAX phase (Figure 1a, Supplementary Table S1). When the combustion temperature is lower than the melting points of the products formed, phase separation does not occur, and alumina-reinforced MAX composites are formed as a result. The Ti-Al-C ternary system was among the most studied ones, containing three phases (as shown in Figure 1b). Ti_3AlC and Ti_2AlC melt incongruently at 1580 and 1625 °C, respectively, producing the liquid-phase, TiC and either Ti_2AlC or Al_4C_3. Typically, Ti_3AlC_2 melts at 1360 °C. More than half of the published works dealt with the synthesis and characterization of the Ti-Al-C ternary system; however, a comparative overview of the results will shed light on the controversial facts regarding these systems.
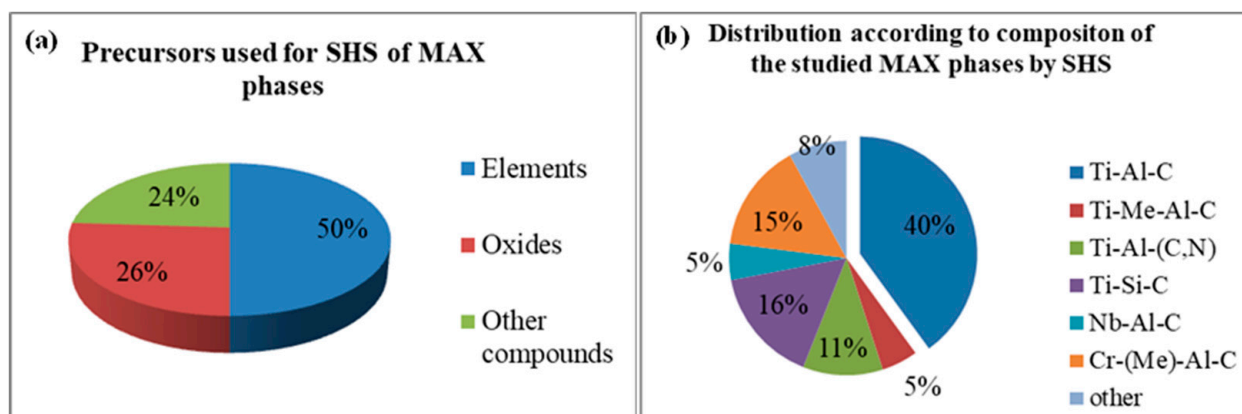
Figure 1. Analysis of the literature available on the SHS-produced MAX phases.

The possibility of a self-sustained reaction was repeatedly confirmed using thermo-dynamic calculations [10]. Enthalpy vs. temperature calculations were presented for the

following reaction scheme: $2Ti + (1 + y)Al + C \rightarrow Ti_2AlC + yAl$, and $T_{ad} \geq 1800$ K and $-\Delta H^{298K}/C_p^{298K} \geq 2000$ K, which was found to be relevant for the preparation of the Ti_2AlC MAX phase under the SHS mode. If excess Al is added it serves as a diluent and decreases T_{ad}; meanwhile, preheating the reactants may allow the elevation of the combustion temperature, offering more flexibility in regulating the exothermicity of the SHS process.

The wet or dry mixing of elements, ball milling or mechanical activation, preheating, and magnetic induction are sometimes accompanied by microwave assistance (MW) or laser induction, and cold pressing to a relative density of up to 60% followed by SHS in a vacuum or Ar atmosphere leads to the mixture of Ti_3AlC_2, Ti_2AlC, and TiC with different wt.% contents depending on the ratio of the elements present in the initial mixture, particle size, apparent density, mechanical activation (MA) duration, etc. In particular, Hendaoui et al. [11] reported the formation of Ti_2AlC with up to 2 wt.% TiC at $T_c = 2000$ K from the stoichiometric mixture, while $T_c = 2194$ °C was registered by the authors of [12] with the formation of Ti_2AlC and Ti_3AlC_2, with the only difference in carbon particle size (<50 μm vs. 1 μm) and initial mixture preparation conditions (Supplementary Table S1). The simultaneous existence of Ti_3AlC_2 and Ti_2AlC from the 2:1:1 stoichiometric mixture of elements could be explained by a possible Ti_2AlC+TiC interaction at 1420 °C [13,14]. The value of isostatic pressure (80 MPa vs. 20 MPa) deserves special attention, since samples that are too dense have too high thermal diffusivity and are poorly ignited; moreover, a higher pressure/loading force prevents the retrieval of the unbroken samples. A 1–5 min MA decreases T_c from 2000 to 1700 °C in the 3:1:2 elementary mixture, respectively, leading to the formation of Ti_3AlC_2 (45%), TiC (34%), and Ti_2AlC (13%) at 5 min of MA. The optimal duration of MA in terms of the maximum heat release was determined as 3 min. It was shown that MA increases the TiC content, while the usage of TiH_2 increases the content of the Ti_3AlC_2 MAX phase after SHS [15,16]. Mechanochemical synthesis of the Ti_3AlC_2 MAX phases, which was initiated following an 8.33 h milling time of the elements under the stoichiometric ratio, led to the formation of the Ti_2AlC_2 and Ti_3AlC_2/TiC samples [16,17]. The authors of these studies found the cooling rate to be beneficial for SHS control, and Al excess to be particularly useful for pure MAX phase formation, respectively. CO_2 laser-induced SHS of the Ti-Al-C system resulted in Ti_2AlC (83 wt.%) and TiC; moreover, Sn additives improved the yield of Ti_2AlC. In the 2Ti/Al/C/0.3Sn mixture, the amount of Ti_2AlC in the sample reached to approximately 95% [18]. The influence of silicon addition and aluminum infiltration was demonstrated during the SHS of Ti_3AlC_2 MAX phase preparation from the loose powder mixture of the elements. Al infiltration reduces MAX content, while Si addition increases it. As a result, Ti_3AlC_2, TiC, Al, $TiAl_3$, and TiAl are formed ($U_c = 6$ mm/s) [19]. Ti_3AlC_2 with TiC > 34% has been produced in the air previously from the cold-pressed elementary mixture. The authors reported an excess of aluminum, using soot instead of graphite, coarse-grained titanium, and higher volume of the sample is beneficial for the purity of the MAX phases, as TiC was formed at the first stage, which then dissolved in Ti-Al at 1400–1500 °C for 4–5 s [20]. The change in the initial porosity of the pellet had negligible impact on the composition, while preheating the initial reaction mixture hampered the formation of the MAX phases in the Ti–Al–C mixture, where Ti_2AlC and Ti_3AlC_2 tend to form along with the TiC and TiAl byproducts [21]. During the process of thermal explosion at 670 °C, the Ti_2AlC amount was up to 90% and some amount of TiC_{1-x} was formed. Here, the authors also claimed that the formation pathway of Ti_2AlC during the cooling stage from the high temperature (>2000 °C) arose due to the peritectic interactions between the already formed liquid Ti-Al (after Al melting) and the solid TiC_{1-x} [22]. The influence of the initial mixture composition (ratio of elements) and the TiC amount on the SHS production of Ti_3AlC_2 and Ti_2AlC was subsequently deduced [23,24]. At $T_c = 1800$ °C, the formation of Ti_3AlC_2 during the cooling stage was observed (along with Ti_2AlC and TiC). It was shown that TiC with an Al-coated core-shell composite will be beneficial for reactive sintering and the SHS of the MAX phases [23]. Ti_2AlC_{1-x} and Ti_3AlC_2 were also prepared by the authors of [25] from the Ti:Al:C = 3:1.5:1 and 2:1:0.7

mixtures. The maximum temperature for the formation of Ti_2AlC_{1-x} was about 1625 ± 10 °C, which was driven by the heat released from the $Ti + C = TiC$ reaction.

The Ti_3SiC_2-Ni composite was prepared from the elements with the Ti:Si:C = 3:1.25:2 ratio via infiltration through the nickel or Ni–Si alloy skeleton. The more homogeneous composite material is formed by alloying 20 wt.% Ni using the Ni–Si alloy. An increase in the Ni content initially increases the content of the byproducts (TiC, $TiSi_2$), and then (>50%) leads to the complete disappearance of the MAX phase due to an insufficient combustion temperature [26].

The MW-assisted combustion synthesis of the elements under a magnetron power of 200–400 W generates Ti_2AlC grains of rather high purity (still including the TiC crystals). The ignition temperature was reached and the synthesis then started at ~670 °C when the melting point of Al was attained, with T_c = 1600 °C. Compact deformation includes axial elongation and radial contraction [27]. SHS-combined grinding was used to obtain Ti_3AlC_2 from the Ti:Al:C = 3:2:1.5 mixture at T_c = 1700 °C, forming the Ti_xAl_y intermetallic compounds and titanium carbide (TiC) as byproducts [28]. To demonstrate the role of the combustion mode, self-sustaining interaction and thermal explosion were comparatively assessed in the Ti-Al-C system (with a 3:1:2 ratio of the elements), with T_c = 1673 °C under the SHS mode and T_{max} = 1528 °C under the explosion mode, respectively. The thermal explosion mode allowed for the production of a purer MAX Ti_3AlC_2 phase (85%) compared to that produced under the wave propagation mode (60%) [29].

Under the SHS compaction of Ti, Al, and the soot mixture (64.2 Ti, 27.1 Al, and 8.7 C wt.%, respectively), a gradient structure was formed (T_c = 1350–1500 °C) comprising two stoichiometric MAX phases: 60 wt.% Ti_3AlC_2 and 10 wt.% Ti_2AlC, as well as rounded TiC grains of 20 wt.% and 10 wt.% of the Ti_5Al_{11} and $TiAl_3$ intermetallic phases of titanium aluminide, respectively [30]. Another strategy that has been put forward is the implementation of SHS in the magnetic field. A T_c = 1500–1600 °C has been registered during the Al-Ti-C porous structure formation from the elementary mixture [31].

It was revealed that despite the stoichiometry of the initial mixture, the heat losses and duration of the mixture spending at a given temperature, the sample diameter, and the amount of powder bed, in other words: fast heating, long dwelling at the given temperature, and fast cooling hold the key to the efficient synthesis of the pure MAX phases. Moreover, for the self-sustained interaction a co-milling of the reactants is required to promote the kinetics of the reaction [11].

Furthermore replacing the M, A, or X atoms have gone beyond the state-of-the-art providing boundless platforms of exploration. The preparation of boron containing the MAX phase by replacing half of the carbon atoms by boron in Ti_3AlC_2 allowed for the production of a partially modified boron-containing MAX phase, where the interplanar distances of the crystal lattice in the Ti_3AlC_2 phases (shifting to lower angles) increase as more carbon atoms are replaced by boron in the charge; TiB, TiB_2, and Al_3Ti become the main phases in the product obtained [32]. M-site solid solutions of $(Ti_{1-x}Nb_x)_2AlC$ (with a trivial amount of TiC) have been prepared using Ti, Nb, Al, and carbon (x = 0.2–0.8) under conditions of mild combustion. The combustion velocity and temperature tended to decrease from 7.6 to 3.6 mm/s and from 1200 to 1057 °C, accompanied with an increasing x from 0.2–0.8, respectively [33], indicating a possible compositional change. However, the authors of this study did not comment on the phase composition dependence on the x value. SHS in the Ti-Si-B system typically lead to the formation of the TiB, TiB_2, and Ti_5Si_3 phases, while TiB, TiB_2, and $AlTi_3$ are formed from the Ti-Al-B system, respectively. The binary borides Ti_3SiB_2, Ti_3AlB_2, and Ti_2AlB, but not MAX phases, were also observed [34].

Ti_3SiC_2, with some TiC, was produced by Pampuch through preheating the elements. The crucible was initially heated to 800 °C, and then was rapidly increased at a rate of 500 K/min to 1050–1200 °C [2]. This work pioneered the research of the next decades. The ignition of a loosely compacted $3Ti + Si + 2C$ powder mixture resulted in the stable propagation of the combustion wave with T_c = 1800 °C. This process led to the formation of the Ti_5Si_3 and Ti-rich TiC_{1-x} phases. The formation of Ti_3SiC_2 took place during the cooling

stage by the process of crystallization from the liquid concurrent with the precipitation of the stoichiometric TiC, which is similar to that observed in the other MAX phases [35]. Field-activated, pressure-assisted combustion in the Ti, Si, and graphite mixture of 3:1:2 ratio propagates with the velocity of 18.8 mm/s, and the measured maximum temperature was determined as 2260 °C (with an adiabatic combustion temperature of 2735 °C). The >98% conversion was attained for the samples held at 1525 °C for 2 h. When the holding time is zero, only TiC may be observed [36]. The single-stage preparation of the Ti_3SiC_2–Cu composite from the 3Ti + 1.25Si + 2C mixture and copper infiltration process was found to be possible in only realizing in the presence of silicon in the copper melt, as the high amount of heat consumes on Cu briquette melting, and thereby does not ensure the required fluidity and wetting [37]. Hence, the influence of silicon excess would be of interest when synthesizing Ti_3SiC_2-based materials. For small batches, a 3Ti + 1.8Si + 2C mixture was found to be optimal as the Ti_3SiC_2 content in the combustion product, attaining a value of 58.4 wt.%, while a higher Si content increases the intermetallic amount. A large-scale SHS reaction leads to the formation of Ti_3SiC_2 (88.2 wt.%) in the case of the stoichiometric reaction [38]. Ti_3SiC_2, with a (12–18) vol% TiC and traces of TiSi and $TiSi_2$, was produced from the elements under a 2100 °C combustion temperature, but only after annealing at 1673 K was a single phase was formed [39]. Nb_2AlC was also successfully produced by the same authors [39] from the elements along with the NbC and Nb_4AlC_3 byproducts. Of note, the formation of Cr_2AlC from their constituents via the combustion synthesis process is not deemed to be feasible due to the insufficient exothermicity of the interaction between Cr, Al, and C. Hence, a Ti:Cr:Al:C = (2 − m):m:1:1 mixture was used to promote the self-propagation reaction, and at m = 0.5, Ti_3AlC_2, TiC_x(x < 1), Cr_2AlC, and Al_8Cr_5 were formed [12]. The influence of Al on the Ta_2AlC SHS process and phase formation was investigated. Excess Al decreases the U_c from 6.5 mm/s (stoichiometric) to 3 mm/s (1.6 mol Al), and the T_c from 1250 to 1050 °C, respectively, but contributed to single-phase Ta_2AlC formation from the mixture of Ta:Al:C = 2:1.6:1 (Al excess by 60%) [40]. The Zr_2SC MAX phase with some ZrC content was produced via SHS from the elementary mixture. Furthermore, it was previously thought that Mo-added Zr_2SC may become the promising material, especially in terms of their solid lubricity. Higher amount of molybdenum prevents the MAX phase formation process in the Zr–S–C system [41]. The MAX phase formation process was investigated in the Zr:Al:C = 2:1:1 system. Even though the maximum combustion temperature was attained 1730 °C, no ternary compounds were detected in the final product [42].

2.2. SHS from Elements and Compounds

As previously implied, there are procedures which not only use elemental powders, but also use compounds or their mixtures (Supplementary Table S1). The influence of Al_4C_3, titanium aluminides, and titanium hydride was deduced by the authors in [15,43]. A TiAl and C mixture was combusted in 1 atm Ar after 6 h milling. Ti_3AlC_2 and TiC were produced at T_c = 1396 °C and U_c = 5.9 mm/s, respectively, which is lower by 200 °C compared to when using elements alone [44]. Of note, a single-phase Ti_2AlC product is more difficult to produce compared to the other ternary phases of the Ti-Al-C system.

The elemental powder compacts of the Ti:Al:C = 3:1:2 ratio and 1.85 to 5.56 mol% Al_4C_3-containing samples were cold pressed after dry mixing and ball milling and were then combusted under an Ar atmosphere. The formation of $T_{i3}AlC_2$, Ti_2AlC, and TiC was observed with the T_c = 1300–1400 °C. It was shown that with an increase in the content of Al_4C_3 accompanied with an increasing apparent density, the combustion temperature and the front propagation rate tended to be reduced; the yield of Ti_3AlC_2 formation was improved [43]. Similar research was performed for the 211 system, which was designed to be aimed for the disclosure of the TiC (6.67–14.3 mol%) and Al_4C_3 (1.96–10 mol%) impacts. The TiC-diluted mixture was found to better than the Al_4C_3-containing mixture in terms of the product purity, i.e., maximum amount of Ti_2AlC (>90 wt.%) was produced under mild combustion conditions (T_c = 1200 °C, U_c = 14.3 mm/s) [45]. Al_4C_3 is hydroscopic;

however, it has a lower vapor pressure than Al. Otherwise, high heating rates are required in order to avoid aluminum melt and become the route of Ti transfer. The fabrication of the $Ti_3(Al_{1-x},Sn_x)C_2$ solid solutions via the SHS method from their constituent elemental powder compacts with Al_4C_3 and TiC additions (x = 0–0.8 mol) occur at combustion temperatures of 1590–1700 °C, with flame propagation speeds of 14.2–18.8 mm/s for the Al_4C_3-added samples, and T_c = 1220–1280 °C and U_c = 7.1–9.6 mm/s for the TiC-adopted samples, respectively. Due to the TiC dilution effect, the extent of Sn substitution for Al to form $Ti_3(Al,Sn)C_2$ is narrower for the TiC-adopted sample (y = 0.6), but wider for the Al_4C_3 sample (x = 0.8). At higher x and y values, phase evolution is unable to be completed due to either the reaction time being too short, or due to the combustion temperature being too low [46].

SHS produced Ti-Al intermetallics serve as affordable precursors for the Ti-Al-C MAX preparation process (of both the 211 and 312 structures) for further densification by hot pressing. In the case of the 211 ratio, the dominating phase comprised Ti_2AlC (95.4 wt.%) with some $TiAl_2$ phase (4.6 wt.%), while the 312 composition led to a 73.8 wt.% of Ti_3AlC_2, 11.3 wt.% of Ti_2AlC, and 14.8 wt.% of TiC, respectively [47]. The use of the TiAl compound significantly reduces the T_c, resulting in the formation of the ternary Ti_3AlC_2, Ti_3AlC, and Ti_2AlC phases [48]. Moreover, it was shown that Ti_3Al usage is more beneficial than TiAl for the Ti_3AlC_2 preparation (the quantity of the MAX phase was doubled in the product) [49].

Materials produced from the Ti-Al-C-N system possess specific heterodesmic structures and exhibit pseudo-plastic properties. In contrast to the carbon-containing MAX phases, a loose powder bed is required for the nitrogen-containing MAX preparation process to promote N_2 penetration into the sample during the combustion wave propagation. Ti_2AlN formation under a low nitrogen pressure from the Ti_3Al and aluminum mixture was prepared [49] and was found to be suitable for the engineering applications. The quaternary $Ti_2AlC_{0.5}N_{0.5}$ system, along with some TiC, TiN, Ti_3Al, and AlN, was prepared from the $Ti–Al_4C_3–Al–AlN$ mixture under a nitrogen atmosphere. It was shown that titanium carbonitride Ti(C,N) dominated in the products synthesized from the $Ti–Al_4C_3–AlN$ mixtures under P_{N2} = 1.48 and 1.82 MPa pressure. Moreover, while the combustion parameters and TiC amount increase under higher pressures, they decrease with the addition of AlN instead of Al [50]. The high-purity Ti_2AlN ceramic, with up to 4 wt.% of TiN, was rapidly synthesized via the thermal explosion process in a >650 °C preheated furnace for 2 min. Moderately excess levels of Ti and/or Al (Ti:Al:TiN = 1.1:1.1:1, 1:1.05:1), smaller particle sizes of TiN, and 2–8 mm heights of the compacts used were found to be beneficial for obtaining high-purity Ti_2AlN. The latter was precipitated during the cooling stage of the TiN-dissolved TiAl melt. Higher excess levels of Ti and Al lead to a high T_{ad} and the decomposition of the MAX phase [51,52]. The charge of the Ti_3Al, Al (+50% Al excess) mixture ignited for 60 s at 1.5–5 atm N_2 pressure contained over a 40 wt.% of the MAX phase [53]. No influence of the pressure of nitrogen was observed in the studied interval. In the work published by the authors of [54], two mole of Ti, one mole of Al, and a 37 wt.% TiAl mixture were used as raw materials under different N_2 pressures to obtain Ti_2AlN via the SHS method. TiN and $AlTi_3$ were present as impurities; the latter disappeared at P = 8 MPa N_2. Ti_2AlN, TiN, and Ti-Al intermetallic formation was observed in the AlN- and TiN-diluted mixtures of Al and Ti. TiN dilution promoted Ti_2AlN formation under low pressure, and AlN under high N_2 pressure, respectively [55]. The hydride cycle (HC) approach of the synthesis of the transition metal hydrides was utilized to obtain Ti_2AlN_x via a two-stage strategy. The first step includes the synthesis of the Ti-N solid solution ($TiN_{0.18}$) and titanium hydridonitride with the formula $TiN_{0.18}H_{1.34}$. Following this, the synthesis of the Ti_2AlN_x MAX phase using the HC technique can be fulfilled according to the reaction: $2TiN_{0.18}H_{1.34} + Al \rightarrow Ti_2AlN_{0.25} + H_2$. It is also possible to prepare the Ti_2Al intermetallic via the HC method according to the reaction: $2TiH_2 + Al \rightarrow Ti_2Al + H_2\uparrow$, and then implement the SHS method according to the following reaction: $Ti_2Al + N_2 \rightarrow Ti_2AlN_{0.63}$ [56]. The (TiB–30 wt.% Ti) mixture modified by up to 5 wt.% AlN dopants obtained by SHS extrusion was found to be very sensitive to the AlN content in terms of the combustion

temperature and phase composition. When the content of AlN is 3 wt.% in the initial charge, it reacts with the titanium matrix during the combustion process with the formation of the Ti_2AlN and Ti_4AlN_3 MAX phases. AlN, at a 5 wt.%, decomposes during combustion accompanied with the release of titanium nitrides and pure aluminum, as well as the TiB, TiB_2, and Ti_2AlN phases [57]. Ceramic nanolaminates of Ti_3SiC_2, Ti_3AlC_2, and Ti_2AlN were produced using TiAl and Ti_3Al under a nitrogen atmosphere. Ti_3Al usage lead to the formation of higher amount of Ti_3AlC_2 than using TiAl. Ti_2AlN formation was accompanied by small amount of TiN, Ti_3AlN, and Ti_3Al [58].

In certain cases, it is required to limit some levels of intermediate formation. Hence, high heating rates are required, and/or compounds may have to be used instead of elements. In order to utilize the 3Ti + SiC + C reactants for Ti_3SiC_2 preparation preheating was implemented (T_{ig} = 870 °C). The final product obtained was of a lower phase purity than that reported by Pampuch et al. (which contained 78%Ti_3SiC_2, 17%TiC_x, and 5%$Ti_5Si_3C_x$, respectively) [2], but the significant reduction observed in the heating rate from 500 °C/min to 30 °C/min, respectively, is a significant advantage [59]. In order to achieve further optimization, the reaction pathway and its kinetics should be thoroughly examined [60]. The MW-assisted SHS method was used to obtain Ti_3SiC_2 preforms of an open porosity in the Ti-SiC-C system (3:1.2:1). The process was initiated by the dissolution of SiC carbide in the Ti particles, resulting in Ti-Si and free C, following which the Ti-Si eutectic reacts with TiC developing a T_c > 1800 °C temperature and leading to the formation of Ti_3SiC_2 [61]. Aqueous solutions of metal nitrates and citric acid can be used to prepare the MAX phase of Cr_2GaC [62]. A small amount of chromium carbide and oxide remained in the final product, and the sample exhibited Pauli paramagnetic behavior and temperature-dependent magnetization.

2.3. SHS Metallothermy

SHS metallothermy, as a promising and efficient alternative process, takes the benefit of the highly exothermic nature of the thermite reaction and the cost-effective merits of the metal oxides as the source of the metallic elements. The detailed procedure is illustrated in Supplementary Table S1. In cases where the propagation of the combustion wave is accompanied with a massive melting of the burned sample, phase separation occurs as a result; otherwise, an alumina-reinforced composite is produced. The Al-TiO_2 thermite reaction in the Ti-Al-C-TiO_2 system allows for the preparation of the Ti_3AlC_2/Al_2O_3 and Ti_2AlC/Al_2O_3 composites under a controllable combustion mode (T_c = 1363 K and U_c = 0.9 mm/s, and T_c = 1313 K and U_c = 0.95 mm/s, respectively). As a result, the secondary-phase TiC is relatively reduced when compared to that formed in the Al_2O_3-free MAX phases [63]. The TiO_2–Mg–Al-C mixture was combusted at a 4–5 MPa Ar pressure in a graphite boat accompanied with the formation of Ti_2AlC, $MgAl_2O_4$, and TiC under the conditions of magnesium deficiency, but an excess of 20–30% Mg amount lead to the formation of Ti_2AlC and TiC mixture. Soot deficiency in the starting mixture reduced the percentage of titanium carbide in the final product and increased the amount of the target product up to 93% [64,65]. In contrast to the work produced by the authors of [20], replacing carbon black by graphite resulted in the formation of well-defined laminate layers of the MAX phases [65]. When increasing the holding time up to 1 h, Ti_3AlC_2 MAX phase formation occurs at 1400 °C, while at 1500 °C, only 5 min is required for the reaction completion. The pressure has been shown to affect the density, but not so much in the composition of the MAX phases [14]. The MAX solid solutions $(Ti_{1-x},V_x)_2AlC$ and $(Cr_{1-y},V_y)_2AlC$ with Al_2O_3 addition were prepared from the $TiO_2/V_2O_5/Al/Al_4C_3$ and $Cr_2O_3/V_2O_5/Al/Al_4C_3$ powder mixtures, respectively. Combustion wave propagation occurred when x > 0.4, and y = 0.1–0.7, as the reduction in the levels of Cr_2O_3 was more energetic than that of TiO_2. Moreover, increasing V_2O_5 increased the combustion temperature, while the reaction front velocity facilitated the evolution of the solid solution and MAX phase formation. The combustion temperature and velocity increased from T_c = 1150–1550 °C and 1.4 to 4.8 mm/s, at x = 0.3–0.7, and from T_c = 1200–1600 °C and 2.2–5.5 mm/s at y = 0.1–0.7, respectively. With the increment of the vanadium content

diffraction peaks of the solid solutions observed shifted to higher angles [66]. Alumina-reinforced $(Ti_{1-x}Nb_x)_2AlC$ solid solutions were prepared from the Ti, Al, Nb_2O_5, and Al_4C_3 mixtures. It was shown that increasing the thermite portion increased the U_c from 4.1 to 11.4 mm/s, and the T_c from 1160 to 1652 °C, respectively, decreasing the Nb_2Al and TiC byproduct amounts as a result [33]. The Nb_2O_5–Al–C mixture, in the presence of the CaO_2–Al high-energy additive, was combusted at a 5 MPa Ar pressure aimed at obtaining the Nb_2AlC MAX phase. The combustion velocity increased from 6 to 12 mm/s, accompanied with an increase in the additive content, while the product yield initially increased from 30 to 67% (with up to 15 wt.% additive), respectively, following which it then subsequently decreased. In all probability, several byproducts play a role of slag, thereby decreasing the combustion temperature [67]. If the T_{ad} = 2870 K and the melting points of Nb_2AlC (2000 K) and Al_2O_3 (2330 K) are lower than that temperature, phase separation occurs. Owing to the density difference between Nb_2AlC (6.5 g/cm^3) and alumina (3.8 g/cm^3), the combustion products are separated into two layers under the force of gravity. At low values of additives (<5%), NbC and Nb_2Al are formed; if additive amounts are already >10%, the MAX phase is formed [68]. $3Nb_2O_{5-x}Al–Al_4C_3$ powder compacts were combusted aimed for the preparation of Nb_2AlC. The formation of Nb2AlC was effectively improved using the samples containing an additional amount Al or Al_4C_3. It was shown that increasing Al from 9 to 13 mol resulted in a decrease in the T_c from 1800 to 1200 °C, and the U_c from 12.5 mm/s to 7.5 mm/s, respectively [69]. Similar research was performed by the authors of [70] on the Cr_2O_3-Al-Al_4C_3 system, which was aimed for the preparation of the alumina-reinforced Cr_2AlC composite. Due to the low exothermicity of the mixture, it was preheated to 300 °C, and spinning combustion modes characteristic to the preheated mixtures was observed, with T_c = 1245 °C and U_c = 3 mm/s. It was revealed that the reaction front velocity increased with the content of Al but decreased with that of Al_4C_3. (Cr,Mn,V)-Al-C MAX phases were also produced from the metallothermic reduction of the corresponding oxides in the presence of the CaO_2+Al exothermic mixture (T_{ad} > 4000 K) [71]. The non-equilibrium character of the $(Cr,V)_2AlC$ solid solution synthesis process from the oxides, aluminum, and carbon due to a short "lifetime" of the melt and its fast cooling and crystallization causes the formation of the vanadium and chromium carbides and intermetallics in addition to the target MAX phases [72]. The presence of impurities in the $(Cr_{0.7}Ti_{0.3})_2AlC$ MAX phases determined by the insufficient lifetime of the melt formed during the combustion wave require further optimization of the post-combustion processes [73]. Instead of using hygroscopic and thermally unstable CrO_3, $CaCrO_4$ as a Cr source was proposed to be utilized in its place [74,75]. The combustion wave in the $CaCrO_4$ + Al + C mixture propagated at U_c = 11 and 7.5 mm/s combustion velocities (with low and high carbon contents) contribute to the formation of Cr_2AlC (67 vol%), chromium carbide (Cr_7C_3) and chromium aluminide (Cr_5Al), whose ratio can be changed by varying the carbon amount in the initial mixture [74], and at certain carbon amount achieve practically single-phase Cr_2AlC [75]. It was demonstrated that an increase in the content of the Cr_2AlC MAX phase in the final product and a decrease in the Cr_5Al_8 and Cr_3C_2 phase contents occur with an increase in the carbon and aluminum contents (to above their stoichiometric proportions) in the initial mixture [76]. Highly pure (according to the XRD patterns obtained) and chemically stable Cr_2AlC was produced via the aluminothermic reductions of the Cr III and Cr VI oxides [76]. It was demonstrated that the addition of excess Al and C accompanied with the increase in the weight of the initial mixture to a hundred grams increases the melt "lifetime" and the conversion degree of the precursors and the intermediates. SHS aluminothermy permitted the preparation of $(Cr,V)_2AlC/Al_2O_3$ with different substitutional proportions using the $(1-x)/2Cr_2O_3-x/2V_2O_5-Al-Al_4C_3$ and $(1-y)Cr-y/2V_2O_5-Al-Al_4C_3$ mixtures. Increasing the proportion of vanadium increased the U_c from 1.3 to 5.5 mm/s and the T_c from 1212 to 1605 °C in the $Cr_2O_3-V_2O_5-Al-Al_4C_3$ mixture at x = 0.1–0.7, respectively, but also allowed for the preparation of the Al_2O_3-added $(Cr_{1-x}V_x)_2AlC$ composites with a wide range of composition (x = 0.1–0.7). In contrary, in the $Cr-V_2O_5-Al-Al_4C_3$ mixtures, drastic increases in the combustion wave velocity

from 2.6 to 12.5 mm/s and T_c = 1400–1670 °C within y = 0.4 − 0.7 $(Cr_{1−y}V_y)_2AlC$) were registered, and y > 0.5 was not observed to lead to formation of the MAX phase due to the high velocity and insufficient reaction time. The authors of this study revealed that the usage of Al_4C_3 instead of carbon is beneficial to prevent the carbothermic reduction of oxide precursors [77]. However, in the work published by the authors of [78], the Ta_2O_5 reduction aluminum metal was demonstrated to be a more effective reducer than Al_4C_3. In particular, elemental Al facilitated the reduction of Ta_2O_5, increased the combustion exothermicity, and improved the evolution of the carbide phases. Combustion velocity for the Ta_2AlC formation reaction was registered 8–14 mm/s depending on the Al, Al_4C_3, and C content; although, it did not prevent MAX phase formation. The SHS process in the $V_2O_5/Mg/Al/C$ mixture in the molten salt NaCl allowed for the production of V_2AlC (95%), Val, VC, MgO, and $MgAl_2O_4$ [79]; however, when using Al as a reducer, only V_2AlC (65 wt.%) was formed with the VC_x, V_2C, Val, and VAl_3 phases [80]. Self-propagating high-temperature synthesis of the cast materials in the Mo-Al-C system was controlled by adding alumina in the initial MoO_3 + Al + C mixture. The largest percentage of Mo_3Al_2C in the ingot was reached at 20% Al_2O_3 [81].

3. Crystal Structure and Microstructure Evolution

Laminated or plate-like microstructure characteristic to the MAX phases was observed for SHS-derived powders or bulks. Several researchers have since mentioned the potential restrictions regarding their more compact lattice structure and the hurdles that are present in the delamination process of the SHS-produced ones. The influence of the initial mixture composition, the combustion conditions, and the dopants have comparatively been discussed below. The basic 211 (one polymorph) and 312 (alfa and beta polymorphs) structures comprise two and three M_6X octahedral layers separating the A layers, respectively, meaning that they share close crystallographic relationships, which provides the possibility of tuning the properties of the multicomponent systems by controlling the microstructures [82,83]. Typically, the 211 and 312 structures have a similar lattice parameter (~3 A), but their c parameters are about 13 and 18 A, respectively (Table 1). With the discovery of the new MAX phases, new microstructures were accordingly manifested; in particular, chemically disordered solid solution MAX phases (in-plane and out-of-plane MAX phases). The correlation between the mechanisms of formation and the evolution of the microstructure has been established wherever relevant. The influence of the heating rate, the combustion temperature, the introduction of the intermediate phases, and the duration of the post-combustion process on the MAX formation process was repeatedly stated. In particular, when comparing the plate-like grains of Ti_3AlC_2 obtained from elements and the Al_4C_3-containing sample, one may note that due to the lower combustion temperature Al_4C_3 contributed to the formation of slightly finer laminates with a size of 5–10 μm. It was also obvious in that several laminated layers were closely stacked in a terraced structure for both of the samples, as shown in Figure 2a,b [43]. It has since been reported more than once in that the high temperature and short reaction time associated with the SHS process are not favorable for the formation of a pure MAX phase. Hence, the selection of a mildly combustible initial mixture composition is a key tool to control both the phase composition and homogeneity of the product. From this perspective, the use of compounds instead of elements for the formation of MAX phases was found to be beneficial. However, during metallothermic reduction, Al_4C_3 caused more significant losses in Al during the combustion compared to that seen with the Al powder.

In the Ti-V-C system, small equiaxed (Ti,V)C grains of about 1–2 μm were formed under a low vanadium content; whereas increasing V in the solid solution grains become laminar and closely stacked into a laminated structure. The Cr-V-C system comprises plate-like $(Cr,V)_2AlC$ grains with a thickness of about 0.2 μm with a laminated feature. Due to substantial melting during the SHS metallothermic process, a dense microstructure of a solid solution composite was formed (as shown in Figure 3a,b).
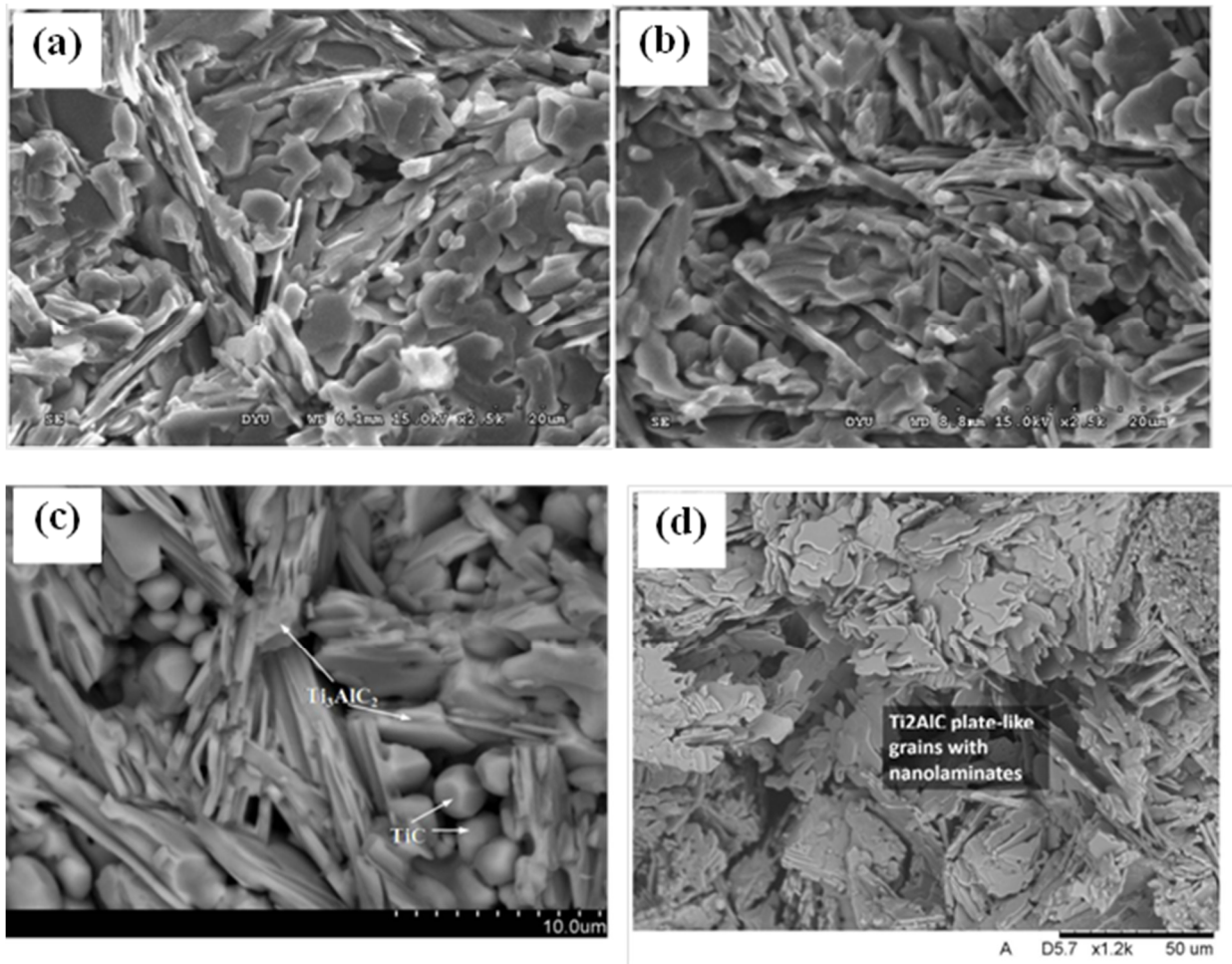
Figure 2. SEM micrographs of the synthesized products obtained from (**a**) an elemental powder compact of 3Ti + Al + 2C and (**b**) a 5.56 mol% Al_4C_3-containing sample of 3Ti + 1.25C + 0.25Al_4C_3. Reproduced with permission [43]. Copyright 2009, Elsevier (**c**) Fracture microstructure of the material synthesized from the MA raw mixture using force SHS-pressing. Reproduced with permission [15]. Copyright 2015, Springer (**d**) SEM image of Ti_2AlC obtained from the elements during the cooling stage of the solid–liquid interaction. Reproduced with permission [27]. Copyright 2016, PTMK.
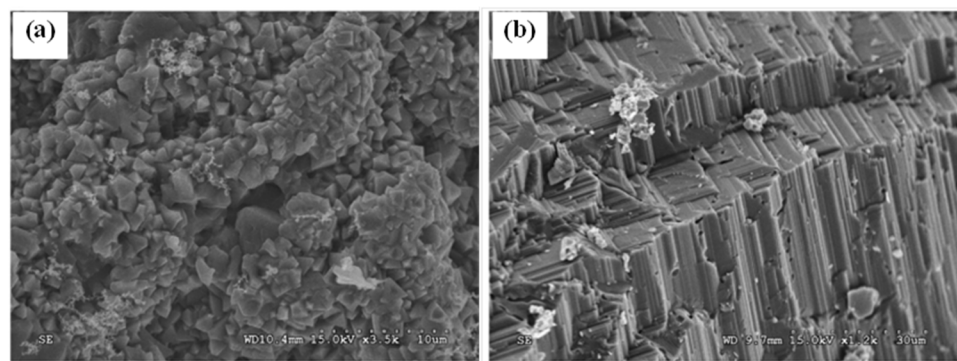
Figure 3. SEM micrographs illustrating the fracture surfaces of the synthesized products of Al_2O_3-added $(Ti_{1-x}V_x)_2AlC$ with x (**a**) 0.3, and (**b**) 0.7, respectively. Reproduced with permission [66]. Copyright 2013, Elsevier.

Cleavage planes typical to the MAX phases were observed in the fracture of the Ti-Al-C system, which turned into rod-like crystals after etching [12].

Ti$_3$AlC$_2$ grains were found to consist of a few superimposed layers, being approximately 0.5 µm in thickness [15]. Up to 16 wt.% circular TiC grains with particles of 3 µm in size were found in the Ti$_3$AlC$_2$ terraced structure (Figure 2c).

Microstructure features have been well discussed by Bai et al. [84]. Ti$_2$AlC bulk pellets obtained via the SHS/PHIP approach comprise plate-like grains of Ti$_2$AlC with a nanolaminated structure (Figure 4c). Flat terraces and surface steps are clearly observed, indicating a step-flow growth mode (which is common mode for MAX), in which the growth rate along the c axis is much lower than the in-plane or a-axis growth rate. The authors further explained that the formation of nanopores can be explained by the accumulation of the carbon vacancies, as carbon atoms do not diffuse adequately in such a short time during the SHS/PHIP process. Increases in the density and grain size were observed with the increasing size of the pellet explained by the slow heat losses (Figure 4a,b) [84], whereas crystal growth was blocked in the small pellet due to the short time designated for heat preservation during SHS [85]. The micron-sized thinner plates contain laminates of a thickness of 50–100 nm, and when the amount of the byproducts increases, mostly rounded particles are observed typical to binary compounds or intermetallics (Figure 4c).
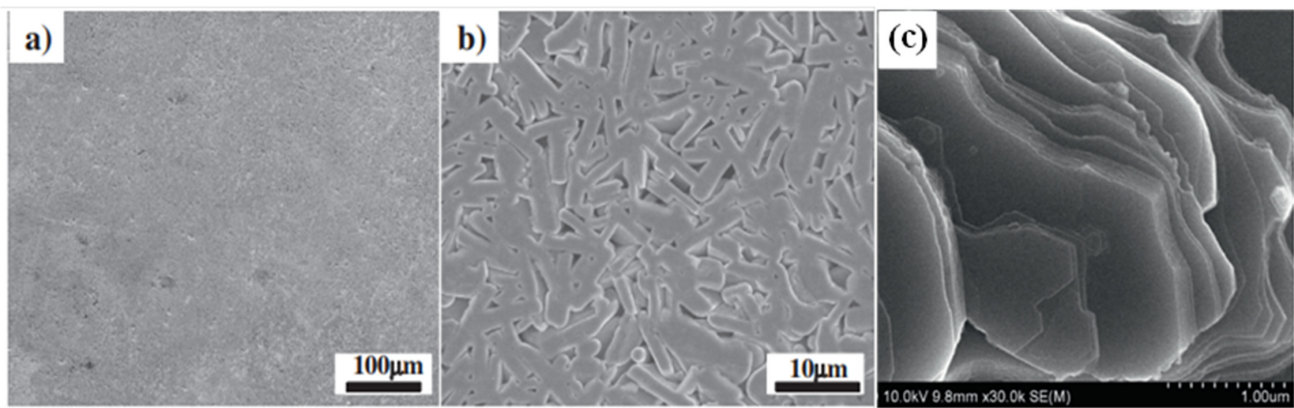
Figure 4. Polished and etched surfaces (**a,b**), and the layered growth of Ti$_2$AlC synthesized by the SHS/PHIP process (**c**) Reproduced with permission [84,85]. Copyright 2014, Elsevier.

The lamellar microstructure is also characteristic to the MAX phases prepared via SHS extrusion [86].

The laminated grains and the terraced structure were observed in Ti$_3$AlC$_2$ sample, regardless of the preparation pathway. Areas marked with rectangles were further enlarged as insets to display the stepped traces in the terraced structure (Figure 5a) [24].

Due to the Al melt, a highly dense (Ti$_3$AlC$_2$–Cr$_2$AlC)-TiC composite with cleavage planes of about 50 nm layer thickness were developed from the mixture of elements (as shown in Figure 5b) [87].

When comparing the microstructure features of the non-activated and mechanoactivated samples from the Ti-Al-C system, one may observe plate-like grains of a similar morphology for both samples, whereas aluminum excess or carbon deficiency are well expressed on the fracture surfaces (small, faceted TiC grains were absent) [16]. The influence of the laser and Sn addition on the Ti-Al-C microstructure was determined to be insignificant, with only a portion of lathed grains having been found to have increased. The average size of the faceted TiC grain was approximately 2 µm. The average length and width of the Ti$_2$AlC lathed grains was 10–20 µm and 2 µm, respectively [18].
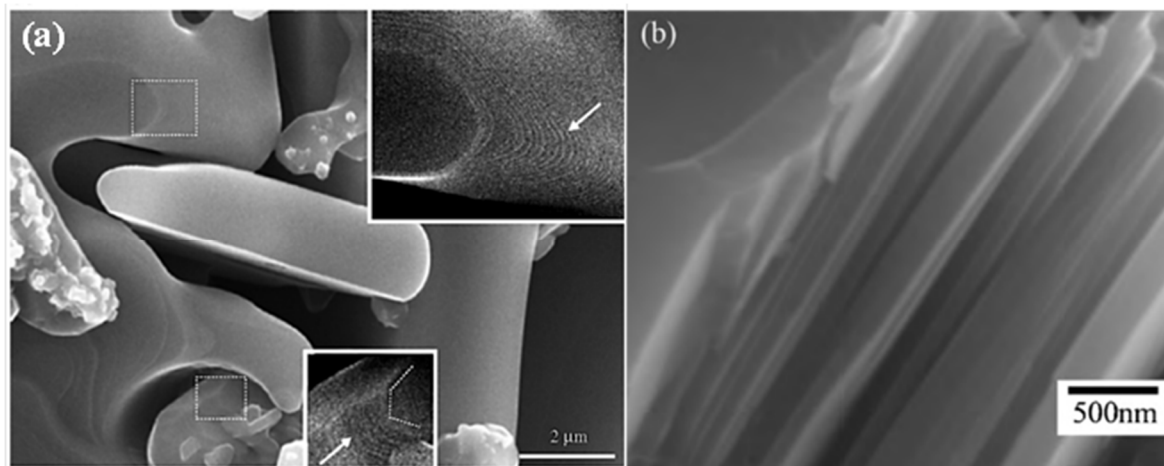
Figure 5. SEM image of the Ti$_3$AlC$_2$ sample with growth steps of grains (**a**) Reproduced with permission [24]. Copyright 2007, Elsevier. SEM image of typical nanolayered structure of (Ti$_3$AlC$_2$–Cr$_2$AlC)-TiC composite SHS/PHIP sample (**b**) Reproduced with permission [87]. Copyright 2010, Elsevier.

Table 1. Lattice parameters (a and c, Å) for the SHS-derived MAX phases.

Sample	a	c	Ref.	Comment
(Ti$_{0.6}$V$_{0.4}$)$_2$AlC	2.998	13.476		
(Ti$_{0.5}$V$_{0.5}$)$_2$AlC	2.981	13.432	[66]	Diffraction lines of (Ti,V)$_2$AlC shift to higher
(Ti$_{0.4}$V$_{0.6}$)$_2$AlC	2.958	13.389		angles with increasing V content
(Ti$_{0.3}$V$_{0.7}$)$_2$AlC	2.946	13.348		
Ti$_2$AlC$_x$,	3.040	13.632		Carbon deficiency caused changes in the
Ti$_3$AlC$_{2x}$,	3.066	18.536	[12]	lattice parameters
Cr$_2$AlC$_x$	2.859	12.768		
Ti$_3$AlC$_2$	3.077	18.593	[15]	Mechanical activation causes minor changes
Ti$_3$AlC$_2$ − MA	3.072	18.567		in the lattice spacing values
Ti$_2$AlC	3.050	13.647	[85]	Considering the high vapor pressure of Al in the raw material at high temperature, it is concluded that the derived material synthesized by SHS-PHIP is non-stoichiometric Ti$_2$AlC$_x$ (x = 0.61445)
Ti$_3$AlC$_2$	3.071	18.536	[87]	Due to the mutual partial displacement of the Ti and Cr atoms in the MAX phases, lattice
Cr$_2$AlC	2.856	12.858		spacing differs from the tabular value.
Ti$_3$AlC$_2$	3.075	18.567	[88]	The relative contraction of the c parameter is 20 times larger than the contraction of the a
Ti$_3$SiC$_2$	3.067	17.672		parameter due to Al substitution by smaller Si
Ti$_3$Al$_{0.5}$Si$_{0.5}$C$_2$	3.072	17.951		atoms in the layered structure
Ti$_3$AlC$_2$	3.072	18.552	[28]	Refined unit cell parameters of the SHS-grinding obtained sample match the literature data for Ti$_3$AlC$_2$ prepared by other methods
Ti$_3$AlC$_2$	3.066	18.525	[89]	
Ti$_3$AlC$_2$	3.071	18.359	[90]	
Ti$_2$AlN$_{0.25}$	2.989	13.654	[56]	Both MAX phases have identical parameters
Ti$_2$AlN$_{0.63}$	2.989	13.654		regardless of the nitrogen content
Cr$_2$AlC	2.86	12.83	[76]	The identical data is indicated in the common databases
Cr$_2$AlC	2.861	12.831	[71]	Manganese content in the MAX phase was not estimated because the dependence of the unit cell parameters of this SS on the Mn content is
(Cr$_x$Mn$_{1−x}$)$_2$AlC	2.855	12.832		obscure.
V$_2$AlC	2.915	13.159	[79]	V2AlC had narrow diffraction lines indicating a high degree of perfection of the crystal structure
Cr$_2$GaC	2.892	12.611	[62]	The product crystallizes in the form of agglomerated anisotropic particles and their morphology differs from the conventionally prepared MAX phases

It should be noted that the lattice parameters of the MAX phases are dependent on the coexisting phases and preparation conditions. In particular, for Ti_3AlC_{1-x} in coexistence with their different secondary phases, a and c vary systematically [91] due to the existence of a homogeneity region. As a matter of fact, the indexing angle decreases with an increase in the lattice parameters if the radius of the solute is larger than that of the solvent atom in the MAX solid solution phases.

Ti_2AlN compacts synthesized by TE at 700 °C for 2 min with 2 and 8 mm heights demonstrate differences in their microstructure. A terraced microstructure was observed when the compact's height was 2 mm, indicating the growth of the Ti_2AlN grains (with the growth along the a-axis being faster than that along the c-axis, respectively) (Figure 6a,b).
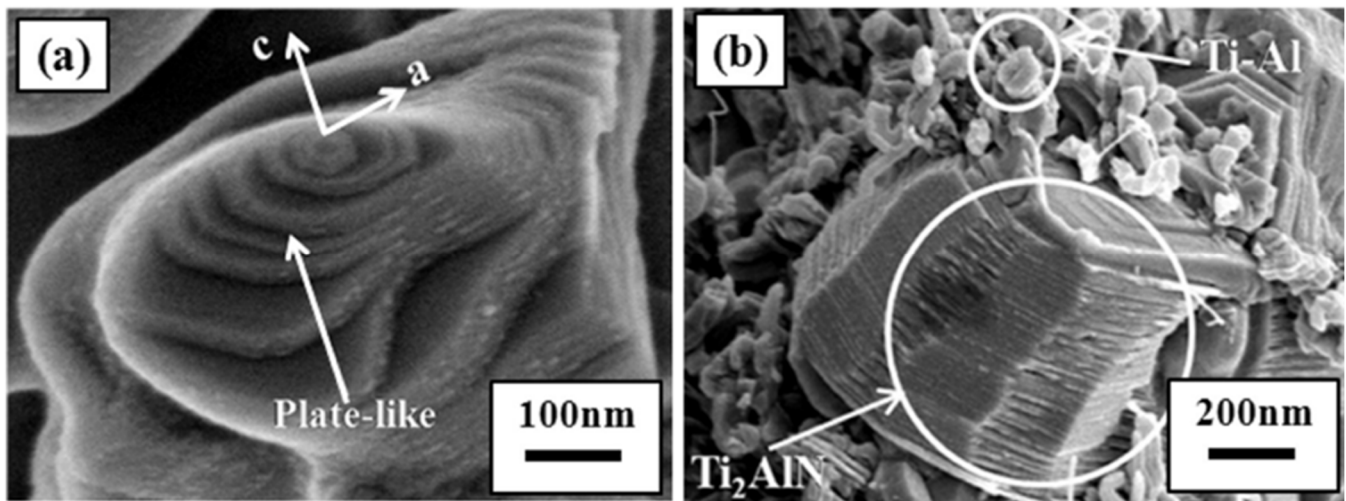
Figure 6. Fractured SEM image of the Ti_2AlN samples obtained by TE with a compact height of 2 (**a**) and 10 (**b**) mm. Reproduced with permission [51]. Copyright 2017, Elsevier.

Moderate (Figure 7a) and complete (Figure 7b) conversion of the samples can also be easily identified in the polished surfaces of the Ti_3SiC_2 pellets produced from the 3Ti + SiC + C mixtures.
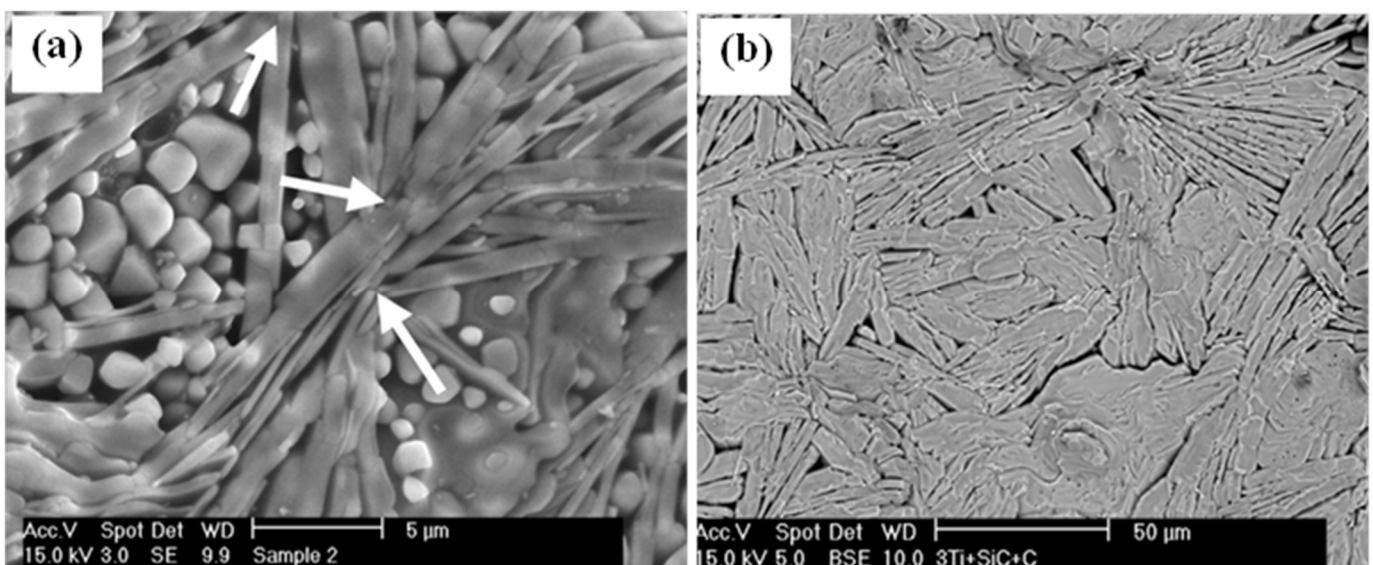
Figure 7. Backscattered electron images of a polished section. (**a**) A closer view of the crystal growth morphology inside a large pore. (**b**) A single phase, plate-like Ti_3SiC_2. Reproduced with permission [59]. Copyright 2003, Springer.

Through the infiltration of nickel into the porous skeleton of the Ti_3SiC_2 MAX phase (Figure 8a vs. Figure 8b), destruction occurs as a result, while the addition of silicon into nickel increases the wettability and promotes the terraced structure formation (Figure 8c). Note that copper infiltration also inhibits the MAX phase formation. In the Cu infiltration region, a large area of destroyed Ti_3SiC_2, consisting of a mixture of TiC and $TiSi_2$ adjoins the Cu area. In the case of 10% Si addition to the Cu briquette, the relative fraction of the Ti_3SiC_2 phase in the resulting composite increased markedly [37].
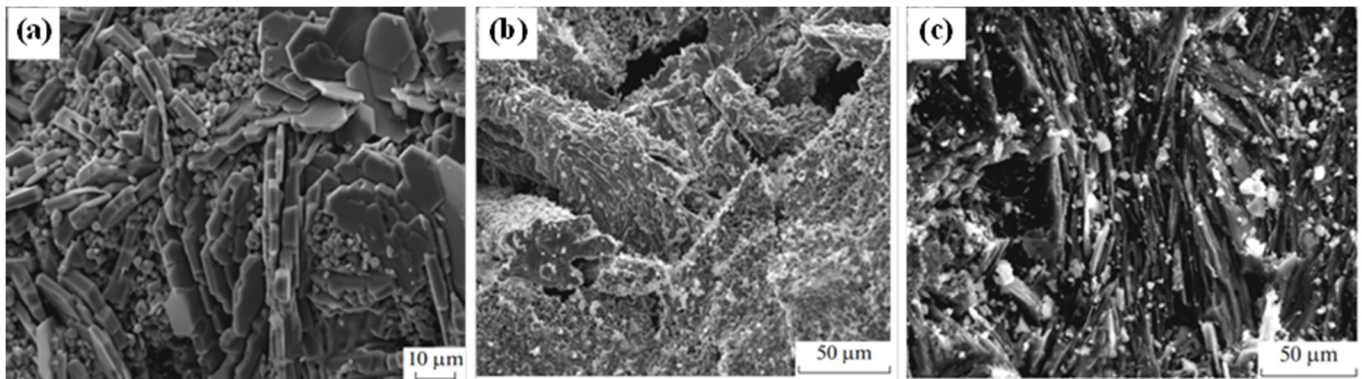
Figure 8. Nickel-uninfiltrated skeleton bottom part (**a**). Nickel-infiltrated top skeleton part (**b**). Bottom Ti_3SiC_2 skeleton infiltrated by Ni-Si (**c**). Reproduced with permission [26]. Copyright 2019, Springer.

Thus, the Ti_3SiC_2 phase consists of elongated plate-like grains, which are connected together in the form of layered nanolaminates usually with the inclusions of TiC, $TiSi_2$, and SiC of a spherical shape [61].

Overall, the microstructure of the MAX phases differs from system to system, while plate-shaped crystals are characteristic to all of them. The influence of the initial mixture composition demonstrated on the example of the Nb-Al-C system reveals the porosity and homogeneity differences according to the carbon content and nitrogen pressure (Figure 9a,b).
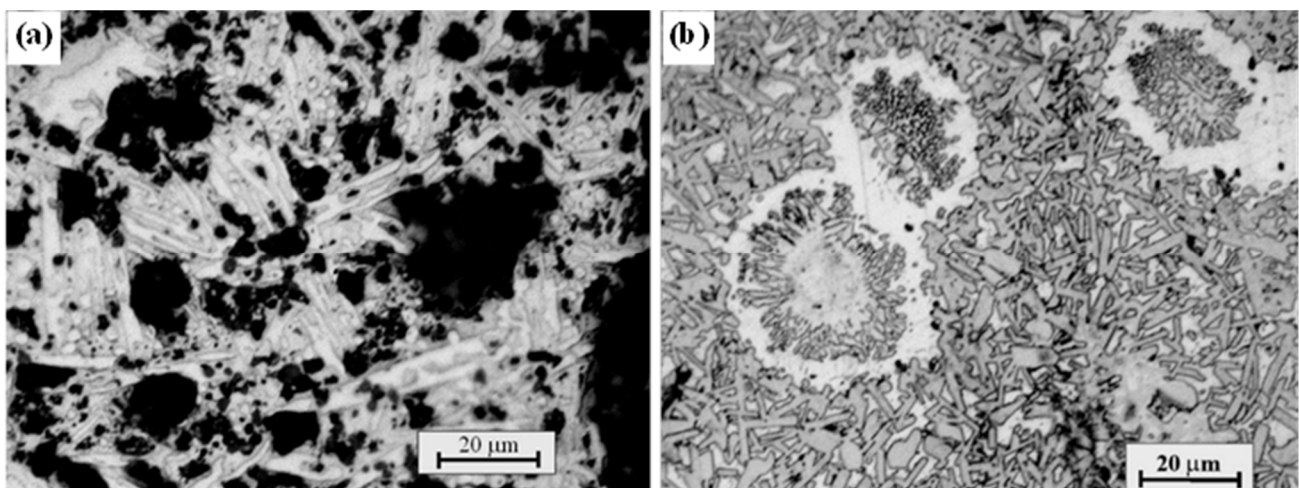
Figure 9. SEM images of 2Nb + Al + C combusted at 6 MPa N_2 pressure (**a**) and 2Nb + Al + 0.5C after SHS in the chemical furnace (**b**) [39].

Aluminothermic reductions of Nb_2O_5 aimed at Nb_2AlC MAX phase preparation showed a clear, dense pellet formation, where the plate-like grains of Nb_2AlC were closely stacked into a laminated structure similar to other MAX phases [69].

The V_2AlC MAX phase obtained via SHS metallothermy consisted of the nanolayered V_2AlC MAX phase and rounded particles of the VC_x phase. The size of the VC_x particles reached 10 μm. At the boundaries of the V_2AlC and VC_x phases, fine inclusions based on the intermetallic VAl_3 and V_5Si_3 phases were observed, as shown in Figure 10a [71]. The Ta_2AlC was also plate-like, consisting of several thin slices with a size of about 5–10 μm, which were closely stacked, entangled, and randomly oriented (Figure 10b) [40].
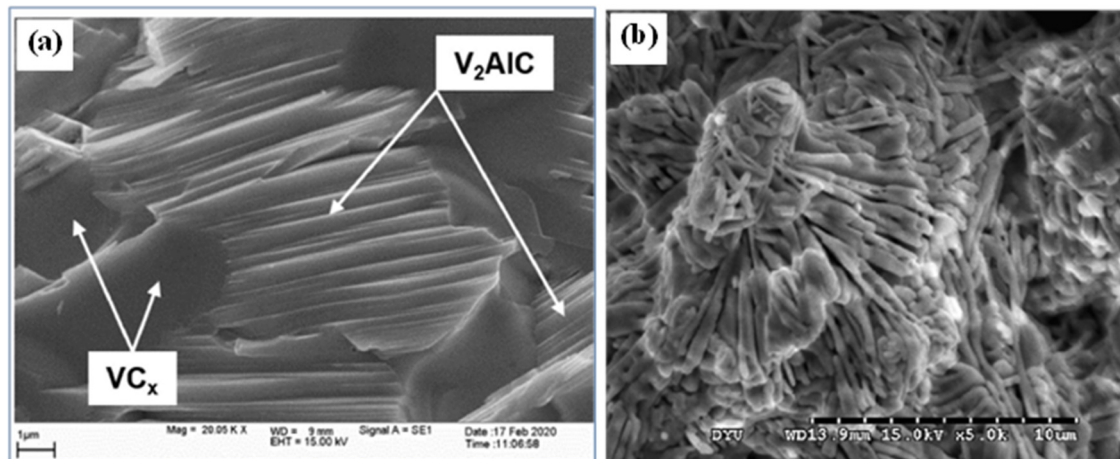
Figure 10. SEM image of the fracture surface of the material based on the V_2AlC MAX phase obtained via SHS metallothermy (Reproduced with permission [71]. Copyright 2021, Elsevier) (**a**) and the Ta_2AlC MAX phase obtained from the powder compact of Ta:Al:C = 2:1.6:1 (Reproduced with permission [40]. Copyright 2009, Elsevier) (**b**).

In general, flake-like plates of a few hundred nm in size are possessed in laminated grains of up to 20 μm in the layered structure of the MAX phases. The terraced microstructure common for these MAX phases evidences that the grain growth is controlled by the solid–liquid interface.

4. Mechanical Properties

Mobile dislocation in the crystal structure endows the MAX phases with machinability, thermal shock resistance, and tolerance to damage. The MAX phases possess the properties of metals and ceramics; they are pseudoductile under high temperatures, but brittle at room temperature. Vickers hardness values of the combustion-synthesized MAX phases range from 2–10 GPa, with fracture toughness of 5–10 $MPam^{1/2}$ (Table 2). Sintering of the MAX phases was simultaneously observed during their synthesis through metallothermic reduction, pseudo-hot isostatic pressing, or pressure-assisted thermal explosion, as well as by hot pressing. Considerable melting of the samples during metallothermic combustion usually leads to the formation of almost fully-dense products. Phase transformation or reactive sintering may occur during the consolidation process, increasing or decreasing the amount of target products depending on the equilibrium of the states established. In particular, SHS-produced samples typically comprise Ti_2AlC and Ti_3AlC_2 (78.1% and 21.9 wt.%, respectively); however, under PHIP, some amount of TiC was observed. In all probability, Al evaporates and/or flows out of the sample under the sintering temperature, and carbon-lean MAX phases are formed along with TiC [66]. The final compact exhibited a 97.09% relative density (4.08 g cm^{-3}) and a Vickers hardness of 4.6 GPa, with the flexural strength being comparatively higher due to the presence of the 312 and 211 phases, while the fracture toughness was comparable to the HP-prepared Ti_2AlC sample [12]. Strengthening of the mechanical properties maybe induced by secondary phase dispersion (TiC, etc.). The MAX phase materials were deemed to be better in the case of Ti_3AlC_2, and weaker in the case of Ti_2AlC.

Table 2. Mechanical properties of the SHS-derived MAX phases.

System	Compaction Method	Density (Theoretical/Relative)	Hardness	Fracture Toughness	Ref.
$(Ti,V)_2AlC/Al_2O_3$	SHS metallothermy	4.12–4.31 g/cm^3	4.8 GPa	7.2 MPam$^{1/2}$	[66]
$(Cr,V)_2AlC/Al_2O_3$		4.53–4.78 g/cm^3	6.3 GPa	9.7 MPam$^{1/2}$	
$Ti_2AlC/Ti_3AlC_2/TiC$	SHS/PHIP	4.08 g/cm^3/97%	4.6 GPa	6.6 MPam$^{1/2}$	[12]
$Cr_2AlC/TiC/Al_8Cr_5/Cr_2Al$		4.64g/cm^3/93%	10.1GPa	5.1 MPam$^{1/2}$	
Ti_2AlC	SHS/HP	2.96g/cm^3/75%	0.62 GPa	-	[47]
Ti_3AlC_2		4.2g/cm^3/99%	4.22 GPa	-	
Ti_2AlC	SHS/PHIP	3.99g/cm^3/98%	-	-	[84]
Ti-Al-C	SHS extrusion	-	4–4.5 GPa	-	[86]
$Ti_2AlC_{0.69}$	SHS/PHIP	97%	5.8 GPa	6.5 MPam$^{1/2}$	[85]
Ti_3AlC_2, Cr_2AlC and TiC	SHS/PHIP	4.55 g/cm^3	10.53 GPa	6.23 MPam$^{1/2}$	[87]
$(Ti_{1-x}Nb_x)_2AlC$ SS	SHS metallothermy	3.4–4.2 g/cm^3	-	-	[33]
$(Ti_{1-x}Nb_x)_2AlC$ SS with alumina		4.3–5.6 g/cm^3	-	-	
$Ti_3(Al,Si)C_2$	SHS/HP	-	-	-	[88]
Ti_2AlC	Pressure assisted TE	98%	6.4 GPa	-	[22]
Ti_2AlN	SHS/HP	4.2 g/cm^3	-	-	[53]
Ti_4AlN_3,Ti_2AlN	SHS/HP	4.6 g/cm^3	-	-	
$Ti_2AlN_{0.25}$	SHS/HC	3.96 g/cm^3	-	-	[56]
$Ti_2AlN_{0.63}$	SHS/HC	3.03 g/cm^3	-	-	
Ti_2AlN and Ti_4AlN_3	SHS extrusion	-	1288–1682 kgf/mm^2	-	[57]
Ti_3SiC_2, TiC	SHS/TE (reactive forging)	>95%	4.6 GPa	-	[22]
Ti_3SiC_2	Field activated pressure assisted SHS	4.53 g/cm^3	6–7 GPa	-	[36]
Ti_3SiC_2	SHS/HP	-	5.8 GPa	7–8.2 MPam$^{1/2}$	[58]
Ti_3SiC_2,TiC	SHS/HP	4.5 g/cm^3	-	-	[38]
Cr_2AlC, Cr_5Al_8	SHS metallothermy	-	412–613 kg/mm^2	-	[71]
$(Cr,V)_2AlC$	SHS metallothermy	-	6.9 GPa	-	[72]
Zr_2SC	SHS	-	2.5 GPa	-	[41]
$Zr_{1.4}Mo_{0.6}SC$	SHS	-	4.0 GPa	-	
V_2AlC	SHS metallothermy	4.85 g/cm^3	-	-	[80]

Ti_3AlC_2 materials prepared from different intermetallic precursors and hot-pressing states under the temperature range of 1300–1450 °C possess an extraordinary set of properties. Increase in the temperature of the hot-pressing process is accompanied with an increase in the TiC content and a higher hardness, thus proving that SHS-derived powders are sinterable and are easy to be subjected to reactive sintering [47]. It is worth to notice that a high porosity may strongly affect the mechanical properties but considering the pre-sintered state of the SHS-derived particles and their propensity to agglomerate, this influence is essentially reduced. Moreover, during the fabrication of the MAX phase via the SHS/PHIP process, most of the plastic deformation occurs under the high pressure applied, affecting the grain shape, residual stress, and deformation behavior, resulting

in a high density of defects [84]. Plate-like grains and laminated structures contribute to high fracture toughness, while fine grains increase the flexural strength and compressive strength, with their nonstoichiometric compositions making them damage tolerant. For example, SHS-prepared, plate-like nonstoichiometric Ti_2AlC_x (x = 0.69) with a grain size of 6 μm demonstrates the highest flexural strength of 432 MPa and a compressive strength of 1037 MPa among other Ti-Al-C phases prepared using different methods [85]. The high hardness of the $(Ti_3AlC_2$–$Cr_2AlC)/TiC$ nano-layered composite was attributed to the presence of the homogenously dispersed TiC and the overlapping joint lamellas of the Ti_3AlC_2–Cr_2AlC phases [87]. The improvement in these mechanical properties can be ascribed to the SHS process features, namely the detention of material at high temperatures in the combustion flame, melting-assisted densification, and controlled cooling behavior. The density of the monolithic $(Ti,Nb)_2AlC$ solid solutions obtained directly from the elements increases with the amount of Nb; however, porous structures are formed, although the melting process that occurs during the aluminothermic reduction of the corresponding oxides promotes a denser structure formation [33]. The TE of the Ti_2AlC sample without pressure leads to porous sample formation, and with a 30 MPa pressure during reactive forging a >98% dense sample was obtained. Here, a significantly higher microhardness value was attributed to the lower conversion of TiC_{1-x} into Ti_2AlC (6.5 GPa vs. 5 GPa for pure Ti_2AlC) [22]. A similar procedure performed for the Ti_3SiC_2 sample under an 80 MPa pressure increased the relative density up to 95%, but also exhibited a lower density compared pure Ti_3SiC_2 due to its higher porosity [35]. The addition of aluminum nitride as a dopant during the Ti-Al-N MAX phase formation gave rise its microhardness due to the dispersion, grain refinement, and homogeneous distribution of the components [57]. Direct comparison of the mechanical properties of the MAX phases is impeded by the significant influence of impurities. For example, covalent inclusions of TiB_2 significantly improve the elastic properties and hardness of the Ti_3SiC_2, whereas SiC deteriorates it. Alumina endows Ti_3SiC_2 with a high damage energy and fracture toughness, but TiC decreases these aspects [58]. Therefore, it is believed that the mechanical properties of the energy-efficient MAX phases prepared by SHS from these affordable precursors are still in their infancy of exploration, and should be thoroughly tested for their potential application, unlike some that have successfully outperformed their counterparts that have been prepared using the traditional methods. In particular, SHS-produced Nb_2AlC ingots and Ti_3AlC_2 bulks have been deemed as promising for their use in conditions of high temperatures and oxidizing environments. Bulk Ti_2AlC exhibited excellent mechanical properties suitable for engineering applications. SHS/PHIP synthesized Ti_2AlC comprises a lot of lattice defects, such as vacancy, dislocation, stacking fault, and grain boundaries resulting in the increased electrical resistivity compared to their bulk counterparts obtained by hot pressing. Ti_3SiC_2 obtained via SHS pressing has been successfully used in electric contacts. SHS-derived Cr_2AlC protective coatings were tested under harsh environments and demonstrated an enhanced behavior. The electrochemical properties of SHS-V_2CT_x were similar to the ones derived by the conventional procedure, suggesting that the scale-up and cost reduction can be achieved by SHS without sacrificing the quality of the material.

5. Summary and Outlook

The influence of the combustion-sensitive parameters (particle size, preheating conditions, sample geometry, packing density, cooling atmosphere, pressure, etc.) on the phase composition, microstructural features, and mechanical properties was discussed in relation to the combustion-synthesized MAX phases. It was established that when using carbon fibers during the SHS process, MAX phase formation cannot be achieved conditioned by rapid cooling. The temperature and velocity of the combustion wave are also higher when graphite is used as a carbon source, and hence soot or carbon black have been determined as the most relevant carbon sources. 'Ti' metal powder with a comparatively lower particle size (∼20 μm) produces several intermetallics and carbides, but coarse-grained Ti allowed for the production of the MAX phase with a higher purity. Some additives lead to the

complete disappearance of the MAX phase, for instance, nickel can impede MAX phase formation caused by poor wettability; in contrast, the Ni–Si alloy promotes the MAX phase formation. It was predicted that high heating rates are required to limit several intermediate formation from elements; however, comprehensive studies revealing the influence of the heating rate are absent in the literature. The usage of compounds, like SiC and TiAl, was uncovered as an alternative perspective for the MAX phase fabrication even at low heating rates. Moreover, large thermal gradients were greatly reduced as compared to the elements. As the cooling stage is mainly responsible for the pure MAX phase formation, different strategies should be developed to control the post-combustion processes and the cooling duration. In terms of the influence of the ambient gas pressure, there are controversial facts; hence, additional studies are required for this factor. The synthesis comprising the steps of solid–solid interactions may be influenced by the cold-pressing conditions. The addition of NaCl and excess reducers (e.g., Al and Mg) to the initial mixture reduces the combustion temperature, promotes the interaction of the components in the inert melt, and increases the yield of the MAX phases. In common with all ternary or quaternary phases, it has proved difficult to synthesize MAX phases without the unwanted "impurity" phases. The properties of these impurity phases (e.g., the TiC_x and Ti_xSi_y types for Ti_3SiC_2) are very different from those of the MAX phase, meaning that they can deteriorate the properties of the MAX phase and hamper the accurate measurements of the mechanical properties. Understanding the mechanisms underlying the formation of the MAX phase across a wide range of temperatures and under programmed heating conditions will contribute to the significant progress in the search for optimal synthesis conditions. As already predicted, the formation of TiAl is expected under low heating rates, whereas high heating rates will contribute to TiC, thereby permitting the control of the purity of target product. Self-propagating high-temperature synthesis is an effective pathway to scale-up the MAX phases from the affordable precursors without energy consumption from the loose and/or dense compacts due to the controllable heating and cooling rates, controllable cooling media, and desired atmosphere. The rapidly growing field of these MAX phases is further expanding to the high-entropy MAX phases, which have already opened up a more diverse platform of new compositions with extraordinary features and targeted applications.

Supplementary Materials: The following supporting information can be downloaded at: https://www.mdpi.com/article/10.3390/cryst13071143/s1, Table S1. Self-propagating high-temperature synthesis protocols of some MAX phases in chronological order.

Data Availability Statement: Data will be made available on request.

Conflicts of Interest: The author declares no conflict of interest.

References

1. Jeitschko, W.; Nowotny, H. Die kristallstruktur von Ti_3SiC_2—Ein neuer komplexcarbid-typ. *Monatshefte Chem.-Chem. Mon.* **1967**, *98*, 329–337. [CrossRef]
2. Pampuch, R.; Lis, J.; Stobierski, L.; Tymkiewicz, M. Solid combustion synthesis of Ti_3SiC_2. *J. Eur. Ceram. Soc.* **1989**, *5*, 283–287. [CrossRef]
3. Barsoum, M.W.; El-Raghy, T. Synthesis and characterization of a remarkable ceramic: Ti_3SiC_2. *J. Am. Ceram. Soc.* **1996**, *79*, 1953–1956. [CrossRef]
4. Sokol, M.; Natu, V.; Kota, S.; Barsoum, M.W. On the chemical diversity of the MAX phases. *Trends Chem.* **2019**, *1*, 210–223. [CrossRef]
5. Zhang, Z.; Duan, X.; Jia, D.; Zhou, Y.; van der Zwaag, S. On the formation mechanisms and properties of MAX phases: A review. *J. Eur. Ceram. Soc.* **2021**, *41*, 3851–3878. [CrossRef]
6. Radovic, M.; Barsoum, M.W. MAX phases: Bridging the gap between metals and ceramics. *Am. Ceram. Soc. Bull.* **2013**, *92*, 20–27.
7. Merzhanov, A.G. History and recent developments in SHS. *Ceram. Int.* **1995**, *21*, 371–379. [CrossRef]
8. Merzhanov, A.G.; Borovinskaya, I.P. Historical retrospective of SHS: An autoreview. *Int. J. Self-Propagating High-Temp. Synth.* **2008**, *17*, 242–265. [CrossRef]

9.   Borovinskaya, I.P.; Gromov, A.A.; Levashov, E.A.; Maksimov, Y.M.; Mukasyan, A.S.; Rogachev, A.S. (Eds.) *Concise Encyclopedia of Self-Propagating High-Temperature Synthesis: History, Theory, Technology, and Products*; Elsevier: Amsterdam, The Netherlands, 2017.

10. Thomas, T.; Bowen, C.R. Thermodynamic predictions for the manufacture of Ti_2AlC MAX-phase ceramic by combustion synthesis. *J. Alloys Compd.* **2014**, *602*, 72–77. [CrossRef]

11. Hendaoui, A.; Andasmas, M.; Amara, A.; Benaldjia, A.; Langlois, P.; Vrel, D. SHS of high-purity MAX compounds in the Ti-Al-C system. *Int. J. Self-Propagating High-Temp. Synth.* **2008**, *17*, 129–135. [CrossRef]

12. Ying, G.-B.; He, X.-D.; Du, S.-Y.; Zhu, C.-C.; Zheng, Y.-T.; Wu, Y.-P.; Wang, C. Formation of $M_{n+1}AX_n$ phases in Ti–Cr–Al–C systems by self-propagating high-temperature synthesis. *Rare Met.* **2014**, *33*, 419–426. [CrossRef]

13. Zhou, A.; Wang, C.-A.; Ge, Z.; Wu, L. Preparation of Ti_3AlC_2 and Ti_2AlC by self-propagating high-temperature synthesis. *J. Mater. Sci. Lett.* **2001**, *20*, 1971–1973. [CrossRef]

14. Wang, X.; Zhou, Y. Solid–liquid reaction synthesis of layered machinable Ti_3AlC_2 ceramic. *J. Mater. Chem.* **2002**, *12*, 455–460. [CrossRef]

15. Potanin, A.; Loginov, P.; Levashov, E.; Pogozhev, Y.; Patsera, E.; Kochetov, N. Effect of mechanical activation on Ti_3AlC_2 MAX phase formation under self-propagating high-temperature synthesis. *Eurasian Chem.-Technol. J.* **2015**, *17*, 233–242. [CrossRef]

16. Hendaoui, A.; Vrel, D.; Amara, A.; Langlois, P.; Andasmas, M.; Guerioune, M. Synthesis of high-purity polycrystalline MAX phases in Ti–Al–C system through mechanically activated self-propagating high-temperature synthesis. *J. Eur. Ceram. Soc.* **2010**, *30*, 1049–1057. [CrossRef]

17. Shahin, N.; Kazemi, S.; Heidarpour, A. Mechanochemical synthesis mechanism of Ti_3AlC_2 MAX phase from elemental powders of Ti, Al and C. *Adv. Powder Technol.* **2016**, *27*, 1775–1780. [CrossRef]

18. Liang, B.; Wang, M.; Li, X.; Sun, S.; Zou, Q.; Mu, Y.; Li, X. Synthesis of Ti_2AlC by laser-induced self-propagating high-temperature sintering. *J. Alloys Compds.* **2010**, *501.1*, L1–L3. [CrossRef]

19. Goc, K.; Prendota, W.; Chlubny, L.; Strączek, T.; Tokarz, W.; Borowiak, P.; Witulska, K.; Bućko, M.; Przewoźnik, J.; Lis, J. Structure, morphology and electrical transport properties of the Ti_3AlC_2 materials. *Ceram. Int.* **2018**, *44*, 18322–18328. [CrossRef]

20. Sun, H.; Kong, X.; Yi, Z.; Wang, Q.; Liu, G. The difference of synthesis mechanism between Ti_3SiC_2 and Ti_3AlC_2 prepared from Ti/M/C (M=Al or Si) elemental powders by SHS technique. *Ceram. Int.* **2014**, *40*, 12977–12981. [CrossRef]

21. Chumakov, Y.A.; Knyazeva, A.G. Combustion synthesis of composite in the Ti-Al-C powders mixture: Model and numerical simulation. *High Temp. Mater. Process. Int. Q. High-Technol. Plasma Process.* **2021**, *25*, 17–35. [CrossRef]

22. Khoptiar, Y.; Gotman, I. Ti_2AlC ternary carbide synthesized by thermal explosion. *Mater. Lett.* **2002**, *57*, 72–76. [CrossRef]

23. Ge, Z.; Chen, K.; Guo, J.; Zhou, H.; Ferreira, J.M.F. Combustion synthesis of ternary carbide Ti_3AlC_2 in Ti–Al–C system. *J. Eur. Ceram. Soc.* **2003**, *23*, 567–574. [CrossRef]

24. Liu, G.; Chen, K.; Zhou, H.; Guo, J.; Ren, K.; Ferreira, J. Layered growth of Ti_2AlC and Ti_3AlC_2 in combustion synthesis. *Mater. Lett.* **2007**, *61*, 779–784. [CrossRef]

25. Chen, K.; Guo, J.; Fu, R.; Ferreira, J.M.F. Combustion synthesis ternary carbide $Ti_2AlC_{1−x}$ powders. *Mater. Sci. Forum* **2004**, *455*, 191–195. [CrossRef]

26. Amosov, A.P.; Latukhin, E.I.; Ryabov, A.M. Applying SHS for the fabrication of the Ti_3SiC_2–Ni composite. *Russ. J. Non-Ferr. Met.* **2019**, *60*, 555–565. [CrossRef]

27. Koniuszewska, A.; Naplocha, K. Microwave assisted self-propagating high-temperature synthesis of Ti_2AlC max phase. *Compos. Theory Pract.* **2016**, *16*, 109–112.

28. Pazniak, A.; Bazhin, P.; Shplis, N.; Kolesnikov, E.; Shchetinin, I.; Komissarov, A.; Polčák, J.; Stolin, A.; Kuznetsov, D. $Ti_3C_2T_x$ MXene characterization produced from SHS-ground Ti_3AlC_2. *Mater. Des.* **2019**, *183*, 108143. [CrossRef]

29. Akhlaghi, M.; Tayebifard, S.A.; Salahi, E.; Asl, M.S.; Schmidt, G. Self-propagating high-temperature synthesis of Ti_3AlC_2 MAX phase from mechanically-activated Ti/Al/graphite powder mixture. *Ceram. Int.* **2018**, *44*, 9671–9678. [CrossRef]

30. Averichev, O.A.; Prokopets, A.D.; Stolin, P.A. Structure formation in Ti/Ti–Al–C layered ceramic materials obtained by the method of unconfined SHS compaction. *Refract. Ind. Ceram.* **2019**, *60*, 219–222. [CrossRef]

31. Dmitruk, A.; Naplocha, K. Development of Al-Ti-C porous structures for reinforcing aluminum matrix composites. *Compos. Theory Pract.* **2022**, *22*, 172–177.

32. Amosov, A.P.; Latukhin, E.I.; Petrov, P.A.; Amosov, E.A.; Novikov, V.A.; Yu, A. Illarionov Self-propagating high-temperature synthesis of boron-containing MAX-phase. *Key Eng. Mater.* **2017**, *746*, 207–213. [CrossRef]

33. Yeh, C.L.; Chen, J.H. Combustion synthesis of $(Ti_{1−x}Nb_x)2AlC$ solid solutions from elemental and Nb2O5/Al4C3-containing powder compacts. *Ceram. Int.* **2011**, *37*, 3089–3094. [CrossRef]

34. Lepakova, O.K.; Karakchieva, N.I.; Golobokov, N.N.; Gal'chenko, N.K.; Afanas'ev, N.I. High-temperature synthesis of Ti–Si–B and Ti–Al–B composites and coatings. *Int. J. Self-Propagating High-Temp. Synth.* **2020**, *29*, 150–156. [CrossRef]

35. Khoptiar, Y.; Gotman, I. Synthesis of dense Ti_3SiC_2-based ceramics by thermal explosion under pressure. *J. Eur. Ceram. Soc.* **2003**, *23*, 47–53. [CrossRef]

36. Feng, A.; Orling, T.; Munir, Z.A. Field-activated pressure-assisted combustion synthesis of polycrystalline Ti_3SiC_2. *J. Mater. Res.* **1999**, *14*, 925–939. [CrossRef]

37. Amosov, A.P.; Latukhin, E.I.; Ryabov, A.M.; Umerov, E.R.; Novikov, V.A. Application of SHS process for fabrication of copper-titanium silicon carbide composite (Cu-Ti_3SiC_2). *J. Phys. Conf. Ser.* **2018**, *1115*, 042003. [CrossRef]

38. Lis, J.; Chlubny, L.; Witulska, K.; Borowiak, P.; Kozak, K.; Misztal, A. SHS of Ti 3 SiC 2-Based Materials in the Ti–Si–C System: Impact of Silicon Excess. *Int. J. Self-Propagating High-Temp. Synth.* **2019**, *28*, 262–265. [CrossRef]

39. Afanasyev, N.I.; Lepakova, O.K.; Kitler, V.D. Non-isothermal synthesis of materials based on the MAX phases in the Ti-Si-C and Nb-Al-C systems. *J. Phys. Conf. Ser.* **2020**, *1459*, 012008. [CrossRef]

40. Yeh, C.L.; Shen, Y.G. Effects of Al content on formation of Ta_2AlC by self-propagating high-temperature synthesis. *J. Alloys Compd.* **2009**, *482*, 219–223. [CrossRef]

41. Inokawa, H.; Ishida, K.; Tomoshige, R.; Hokamoto, K.; Tanaka, S. Effect of Added Molybdenum on Material Properties of Zr_2SC MAX Phase Produced by Self-Propagating High Temperature Synthesis. *Mater. Res. Proc.* **2019**, *13*, 79–84.

42. Kovalev, D.Y.; Luginina, M.A.; Vadchenko, S.G. X-ray diffraction study of self-propagating high-temperature synthesis in the Zr–Al–C system. *Russ. J. Inorg. Chem.* **2017**, *62*, 1638–1644. [CrossRef]

43. Yeh, C.L.; Shen, Y.G. Effects of using Al_4C_3 as a reactant on formation of Ti_3AlC_2 by combustion synthesis in SHS mode. *J. Alloys Compd.* **2009**, *473*, 408–413. [CrossRef]

44. Łopaciński, M.; Puszynski, J.; Lis, J. Synthesis of ternary titanium aluminum carbides using self-propagating high-temperature synthesis technique. *J. Am. Ceram. Soc.* **2001**, *84*, 3051–3053. [CrossRef]

45. Yeh, C.L.; Shen, Y.G. Effects of TiC and Al_4C_3 addition on combustion synthesis of Ti_2AlC. *J. Alloys Compd.* **2009**, *470*, 424–428. [CrossRef]

46. Yeh, C.-L.; Chiang, C.H. Combustion synthesis of MAX phase solid solution $Ti_3(Al, Sn)C_2$. *Nano Hybrids Compos.* **2017**, *16*, 73–76. [CrossRef]

47. Chlubny, L.; Lis, J.; Chabior, K.; Chachlowska, P.; Kapusta, C. Processing and properties of MAX phases–based materials using SHS technique. *Arch. Metall. Mater.* **2015**, *60*, 859–863. [CrossRef]

48. Wang, X.H.; Zhou, Y.C. Layered machinable and electrically conductive Ti_2AlC and Ti_3AlC_2 ceramics: A review. *J. Mater. Sci. Technol.* **2010**, *26*, 385–416.

49. Chlubny, L.; Lis, J.; Bućko, M.M. SHS Synthesis of the Materials in the Ti-Al-CN System Using Intermetallics. *Adv. Sci. Technol.* **2006**, *45*, 1047–1051.

50. Yeh, C.L.; Kuo, C.W.; Wu, F.S. Formation of $Ti_2AlC_{0.5}N_{0.5}$ solid solutions by combustion synthesis of Al_4C_3-containing samples in nitrogen. *J. Alloys Compd.* **2010**, *508*, 324–328. [CrossRef]

51. Liu, Y.; Li, Y.; Li, F.; Cui, H.; Zhang, L.; Guo, S. Synthesis and microstructure of Ti_2AlN ceramic by thermal explosion. *Ceram. Int.* **2017**, *43*, 13618–13621. [CrossRef]

52. Liu, Y.; Zhang, L.; Xiao, W.; Zhang, L.; Pu, Y.; Guo, S. Rapid synthesis of Ti_2AlN ceramic via thermal explosion. *Mater. Lett.* **2015**, *149*, 5–7. [CrossRef]

53. Chlubny, L.; Lis, J.; Borowiak, P.; Chabior, K.; Zieleńska, K. Densification and Phase Evolution of SHS Derived Ti_2AlNActive Precursor Powders During Hot Pressing Processes. *Dev. Strateg. Ceram. Mater. II Ceram. Eng. Sci. Proc.* **2017**, *37*, 211–221.

54. Tian, J.; Zhai, F.; Zhang, L.; Liu, G.; Ding, Z. Effect of N_2 pressure on the phase composition and morphology of Ti_2AlN prepared by self-propagating combustion method. *Adv. Mater. Res.* **2013**, *710*, 199–202. [CrossRef]

55. Yeh, C.-L.; Kuo, C.-W.; Wu, F.-S. Formation of Ti_2AlN by Solid–Gas Combustion Synthesis with AlN-and TiN-Diluted Samples in Nitrogen. *Int. J. Appl. Ceram. Technol.* **2010**, *7*, 730–737. [CrossRef]

56. Aleksanyan, A.G.; Dolukhanyan, S.K.; Mayilyan, D.G.; Muradyan, G.N.; Ter-Galstyan, O.P.; Mnatsakanyan, N.L. Formation of Ti_2AlN_x MAX phase by "Hydride Cycle" and SHS methods. *Ceram. Int.* **2022**, *49*, 24229–24234. [CrossRef]

57. Bolotskaia, A.V.; Mikheev, M.V.; Bazhin, P.M.; Stolin, A.M. The influence of aluminum nitride nanoparticles on the structure, phase composition, and properties of TiB/Ti-based materials obtained by SHS extrusion. *Inorg. Mater. Appl. Res.* **2019**, *10*, 1191–1195. [CrossRef]

58. Lis, J.; Chlubny, L.; Łopaciński, M.; Stobierski, L.; Bućko, M.M. Ceramic nanolaminates—Processing and application. *J. Eur. Ceram. Soc.* **2008**, *28*, 1009–1014. [CrossRef]

59. Riley, D.P.; Kisi, E.H.; Wu, E.; McCallum, A. Self-propagating high-temperature synthesis of Ti_3SiC_2 from $3Ti^+ SiC^+$ C reactants. *J. Mater. Sci. Lett.* **2003**, *22*, 1101–1104. [CrossRef]

60. Riley, D.P.; Kisi, E.H.; Hansen, T.C.; Hewat, A.W. Self-propagating high-temperature synthesis of Ti_3SiC_2: I, Ultra-High-speed neutron diffraction study of the reaction mechanism. *J. Am. Ceram. Soc.* **2002**, *85*, 2417–2424. [CrossRef]

61. Dmitruk, A.; Naplocha, K.; Lagos, M.; Egizabal, P.; Grzęda, J. Microwave assisted self-propagating high-temperature synthesis of Ti_3SiC_2 MAX phase. *Compos. Theory Pract.* **2018**, *18*, 241–244.

62. Siebert, J.P.; Bischoff, L.; Lepple, M.; Zintler, A.; Molina-Luna, L.; Wiedwald, U.; Birkel, C.S. Sol–gel based synthesis and enhanced processability of MAX phase Cr_2GaC. *J. Mater. Chem. C* **2019**, *7*, 6034–6040. [CrossRef]

63. Yeh, C.L.; Kuo, C.W.; Chu, Y.C. Formation of Ti_3AlC_2/Al_2O_3 and Ti_2AlC/Al_2O_3 composites by combustion synthesis in Ti–Al–C–TiO_2 systems. *J. Alloys Compd.* **2010**, *494*, 132–136. [CrossRef]

64. Vershinnikov, V.I.; Kovalev, D.Y. Preparation of Ti_2AlC and Ti_3AlC_2 MAX Phases by Self-Propagating High-Temperature Synthesis with the Reduction Stage. *Russ. J. Non-Ferr. Met.* **2020**, *61*, 554–558. [CrossRef]

65. Vershinnikov, V.I.; Kovalev, D.Y. Synthesis of the Ti_2AlC MAX phase with a reduction step via combustion of a $TiO^{2+} Mg^+ Al^+$ C mixture. *Inorg. Mater.* **2018**, *54*, 949–952. [CrossRef]

66. Yeh, C.L.; Yang, W.J. Formation of MAX solid solutions $(Ti,V)_2AlC$ and $(Cr,V)_2AlC$ with Al_2O_3 addition by SHS involving aluminothermic reduction. *Ceram. Int.* **2013**, *39*, 7537–7544. [CrossRef]

67. Kovalev, I.D.; Miloserdov, P.A.; Gorshkov, V.A.; Kovalev, D.Y. Synthesis of Nb$_2$AlC MAX phase by SHS metallurgy. *Russ. J. Non-Ferr. Met.* **2020**, *61*, 126–131. [CrossRef]

68. Miloserdov, P.A.; Gorshkov, V.A.; Kovalev, I.D.; Kovalev, D.Y. High-temperature synthesis of cast materials based on Nb$_2$AlC MAX phase. *Ceram. Int.* **2019**, *45*, 2689–2691. [CrossRef]

69. Yeh, C.L.; Kuo, C.W. An investigation on formation of Nb$_2$AlC by combustion synthesis of Nb$_2$O5–Al–Al$_4$C$_3$ powder compacts. *J. Alloys Compd.* **2010**, *496*, 566–571. [CrossRef]

70. Yeh, C.L.; Kuo, C.W. Effects of Al and Al$_4$C$_3$ contents on combustion synthesis of Cr$_2$AlC from Cr$_2$O$_3$–Al–Al$_4$C$_3$ powder compacts. *J. Alloys Compd.* **2011**, *509*, 651–655. [CrossRef]

71. Gorshkov, V.A.; Miloserdov, P.A.; Khomenko, N.Y.; Miloserdova, O.M. High-temperature synthesis of composite materials based on (Cr, Mn, V)–Al–C MAX phases. *Ceram. Int.* **2021**, *47*, 25821–25825. [CrossRef]

72. Gorshkov, V.A.; Miloserdov, P.A.; Karpov, A.V.; Shchukin, A.S.; Sytschev, A.E. Investigation of the composition and properties of a Cr$_2$AlC MAX phase-based material prepared by metallothermic SHS. *Phys. Met. Metallogr.* **2019**, *120*, 471–475. [CrossRef]

73. Gorshkov, V.A.; Khomenko, N.Y.; Kovalev, D.Y. The Synthesis of Cast Materials Based on the MAX Phases in a Cr–Ti–Al–C System. *Russ. J. Non-Ferr. Met.* **2021**, *62*, 732–739. [CrossRef]

74. Gorshkov, V.A.; Karpov, A.V.; Kovalev, D.Y.; Sychev, A.E. Synthesis, Structure and Properties of Material Based on V$_2$AlC MAX Phase. *Phys. Met. Metallogr.* **2020**, *121*, 765–771. [CrossRef]

75. Miloserdov, P.A.; Yukhvid, V.I.; Gorshkov, V.A.; Kovalev, I.D. Aluminothermic SHS in CaCrO$_4$–Al–C Mixtures under Nitrogen Pressure. *Int. J. Self-Propagating High-Temp. Synth.* **2018**, *27*, 123–126. [CrossRef]

76. Gorshkov, V.A.; Miloserdov, P.A.; Luginina, M.A.; Sachkova, N.V.; Belikova, A.F. High-temperature synthesis of a cast material with a maximum content of the MAX phase Cr$_2$AlC. *Inorg. Mater.* **2017**, *53*, 271–277. [CrossRef]

77. Yeh, C.L.; Yang, W.J. Effects of co-reduction of Cr$_2$O$_3$ and V$_2$O$_5$ on combustion synthesis of (Cr$_{1-x}$V$_x$)$_2$AlC/Al$_2$O$_3$ solid solution composites. *J. Alloys Compd.* **2014**, *608*, 292–296. [CrossRef]

78. Yeh, C.L.; Chen, Y.S. Effects of Al content on formation of TaC, Ta$_2$C, and Ta$_2$AlC by combustion synthesis with aluminothermic reactions. *Ceram. Int.* **2017**, *43*, 15659–15665. [CrossRef]

79. Vershinnikov, V.I.; Kovalev, D.Y. Formation of V$_2$AlC MAX phase by SHS involving magnesium reduction of V$_2$O$_5$. *Ceram. Int.* **2023**, *49*, 6063–6067. [CrossRef]

80. Gorshkov, V.A.; Miloserdov, P.A.; Sachkova, N.V. High-Temperature Synthesis of Cast Materials Based on the MAX Phase Cr$_2$AlC Using CaCrO$_4$+ Al+ C Mixtures. *Inorg. Mater.* **2020**, *56*, 321–327. [CrossRef]

81. Kovalev, D.Y.; Gorshkov, V.A.; Boyarchenko, O.D. High-Temperature Synthesis of Mo$_3$Al$_2$C-Based Materials via Combustion of MoO$_3$+ Al+ C+ Al$_2$O$_3$ Powder Mixtures. *Inorg. Mater.* **2022**, *58*, 939–947. [CrossRef]

82. Jiang, Q.; Lei, Y.; Liang, H.; Xi, K.; Xia, C.; Alshareef, H.N. Review of MXene electrochemical microsupercapacitors. *Energy Storage Mater.* **2020**, *27*, 78–95. [CrossRef]

83. Rakhadilov, B.K.; Maksakova, O.V.; Buitkenov, D.B.; Kylyshkanov, M.K.; Pogrebnjak, A.D.; Antypenko, V.P.; Konoplianchenko, Y.V. Structural-phase and tribo-corrosion properties of composite Ti$_3$SiC$_2$/TiC MAX-phase coatings: An experimental approach to strengthening by thermal annealing. *Appl. Phys. A* **2022**, *128*, 145. [CrossRef]

84. Bai, Y.; Zhang, H.; He, X.; Zhu, C.; Wang, R.; Sun, Y.; Chen, G.; Xiao, P. Growth morphology and microstructural characterization of nonstoichiometric Ti$_2$AlC bulk synthesized by self-propagating high temperature combustion synthesis with pseudo hot isostatic pressing. *Int. J. Refract. Met. Hard Mater.* **2014**, *45*, 58–63. [CrossRef]

85. Bai, Y.; He, X.; Li, Y.; Zhu, C.; Zhang, S. Rapid synthesis of bulk Ti$_2$AlC by self-propagating high temperature combustion synthesis with a pseudo–hot isostatic pressing process. *J. Mater. Res.* **2009**, *24*, 2528–2535. [CrossRef]

86. Stolin, A.M.; Bazhin, P.M. Manufacture of multipurpose composite and ceramic materials in the combustion regime and high-temperature deformation (SHS extrusion). *Theor. Found. Chem. Eng.* **2014**, *48*, 751–763. [CrossRef]

87. Ying, G.; He, X.; Li, M.; Li, Y.; Du, S. Synthesis and mechanical properties of nano-layered composite. *J. Alloys Compd.* **2010**, *506*, 734–738. [CrossRef]

88. Goc, K.; Przewoźnik, J.; Witulska, K.; Chlubny, L.; Tokarz, W.; Strączek, T.; Michalik, J.M.; Jurczyk, J.; Utke, I.; Lis, J.; et al. Structure, Morphology, Heat Capacity, and Electrical Transport Properties of Ti$_3$(Al, Si)C$_2$ Materials. *Materials* **2021**, *14*, 3222. [CrossRef]

89. Zhu, C.-C.; Zhu, J.; Wu, H.; Lin, H. Synthesis of Ti$_3$AlC$_2$ by SHS and thermodynamic calculation based on first principles. *Rare Met.* **2015**, *34*, 107–110. [CrossRef]

90. Kong, F.; He, X.; Liu, Q.; Qi, X.; Zheng, Y.; Wang, R.; Bai, Y. Effect of Ti$_3$AlC$_2$ precursor on the electrochemical properties of the resulting MXene Ti$_3$C$_2$ for Li-ion batteries. *Ceram. Int.* **2018**, *44*, 11591–11596. [CrossRef]

91. Pietzka, M.A.; Schuster, J.C. Summary of constitutional data on the aluminum-carbon-titanium system. *J. Phase Equilibria* **1994**, *15*, 392–400. [CrossRef]